Article

Immunity

Reactive Neutrophil Responses Dependent on the Receptor Tyrosine Kinase c-MET Limit Cancer Immunotherapy

Graphical Abstract

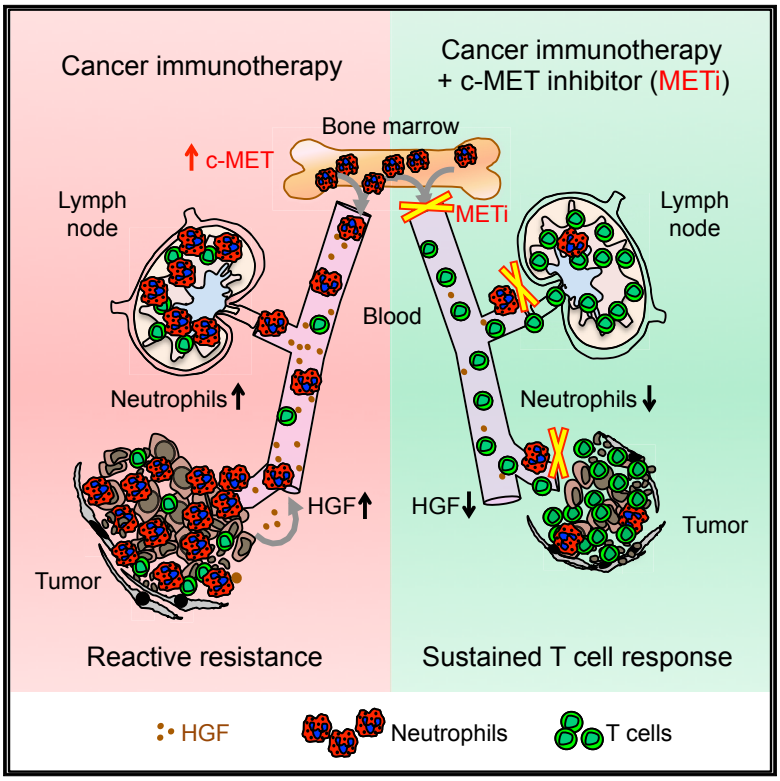

Highlights

- HGF/c-MET signaling mobilizes neutrophils in response to cancer immunotherapies
- Neutrophils acquire immunosuppressive properties in T cell-inflamed tissues
- c-MET^{+} neutrophils suppress therapy-induced T cell expansion and effector functions
- Concomitant c-MET inhibition enhances the efficacy of cancer immunotherapies

Authors

Nicole Glodde, Tobias Bald, Debby van den Boorn-Konijnenberg, ..., Mark J. Smyth, Thomas Tüting, Michael Hölzel

Correspondence

tobias.bald@qimrberghofer.edu.au (T.B.), thomas.tueting@med.ovgu.de (T.T.), michael.hoelzel@ukbonn.de (M.H.)

In Brief

Inhibitors of the receptor tyrosine kinase c-MET are currently used in the clinic to target oncogenic signaling in tumor cells. Glodde et al. now show that c-MET inhibition impairs reactive neutrophil recruitment to tumors and lymph nodes, potentiating T cell anti-tumor immunity. Thus, c-MET inhibitor co-treatment may improve responses to cancer immunotherapy in settings beyond c-MET-dependent tumors.

Glodde et al., 2017, Immunity *47*, 789–802
October 17, 2017
https://doi.org/10.1016/j.immuni.2017.09.012

CellPress

Immunity
Article

Reactive Neutrophil Responses Dependent on the Receptor Tyrosine Kinase c-MET Limit Cancer Immunotherapy

Nicole Glodde,[1,2,3,20] Tobias Bald,[1,2,4,20,*] Debby van den Boorn-Konijnenberg,[3] Kyohei Nakamura,[4] Jake S. O'Donnell,[4,5,6] Sabrina Szczepanski,[7] Maria Brandes,[7] Sarah Eickhoff,[8] Indrajit Das,[4] Naveen Shridhar,[1,2] Daniel Hinze,[3] Meri Rogava,[1,2] Tetje C. van der Sluis,[1,2] Janne J. Ruotsalainen,[1,2] Evelyn Gaffal,[1,2] Jennifer Landsberg,[2] Kerstin U. Ludwig,[9,10] Christoph Wilhelm,[11] Monika Riek-Burchardt,[12] Andreas J. Müller,[12,13] Christoffer Gebhardt,[14] Richard A. Scolyer,[15,16] Georgina V. Long,[16] Viktor Janzen,[7] Michele W.L. Teng,[5,6] Wolfgang Kastenmüller,[8] Massimiliano Mazzone,[17,18] Mark J. Smyth,[4,6] Thomas Tüting,[1,2,19,*] and Michael Hölzel[3,19,21,*]

[1]Laboratory of Experimental Dermatology, Department of Dermatology, University of Magdeburg, 39120 Magdeburg, Germany
[2]Laboratory of Experimental Dermatology, Department of Dermatology and Allergy, University of Bonn, 53105 Bonn, Germany
[3]Unit for RNA Biology, Department of Clinical Chemistry and Clinical Pharmacology, University of Bonn, 53105 Bonn, Germany
[4]Immunology in Cancer and Infection Laboratory, QIMR Berghofer Medical Research Institute, Herston, QLD 4006, Australia
[5]Cancer Immunoregulation and Immunotherapy Laboratory, QIMR Berghofer Medical Research Institute, Herston, QLD 4006, Australia
[6]School of Medicine, The University of Queensland, Herston, QLD 4006, Australia
[7]Department of Internal Medicine III, Hematology/Oncology/Rheumatology, University of Bonn, 53105 Bonn, Germany
[8]Laboratory for Cellular Interactions and Immunimaging, Institute of Experimental Immunology, University of Bonn, 53105 Bonn, Germany
[9]Institute of Human Genetics, University of Bonn, 53127 Bonn, Germany
[10]Department of Genomics, Life & Brain Center, University of Bonn, 53127 Bonn, Germany
[11]Unit for Immunopathology, Department of Clinical Chemistry and Clinical Pharmacology, University of Bonn, 53105 Bonn, Germany
[12]Institute of Molecular and Clinical Immunology, University of Magdeburg, 39120 Magdeburg, Germany
[13]Helmholtz Centre for Infection Research (HZI), 38124 Braunschweig, Germany
[14]Skin Cancer Unit, German Cancer Research Center, Heidelberg and Department of Dermatology, Venereology and Allergology, University Medical Center Mannheim, Ruprecht Karl University of Heidelberg, 69121 Heidelberg, Germany
[15]Department of Tissue Pathology and Diagnostic Oncology, Royal Prince Alfred Hospital, Sydney, NSW 2050, Australia
[16]Melanoma Institute Australia and Sydney Medical School, The University of Sydney, Sydney, NSW 2065, Australia
[17]Laboratory of Molecular Oncology and Angiogenesis, Vesalius Research Center, VIB, Leuven B3000, Belgium
[18]Laboratory of Molecular Oncology and Angiogenesis, Vesalius Research Center, Department of Oncology, KU Leuven, Leuven B3000, Belgium
[19]Senior author
[20]These authors contributed equally
[21]Lead Contact
*Correspondence: tobias.bald@qimrberghofer.edu.au (T.B.), thomas.tueting@med.ovgu.de (T.T.), michael.hoelzel@ukbonn.de (M.H.)
https://doi.org/10.1016/j.immuni.2017.09.012

SUMMARY

Inhibitors of the receptor tyrosine kinase c-MET are currently used in the clinic to target oncogenic signaling in tumor cells. We found that concomitant c-MET inhibition promoted adoptive T cell transfer and checkpoint immunotherapies in murine cancer models by increasing effector T cell infiltration in tumors. This therapeutic effect was independent of tumor cell-intrinsic c-MET dependence. Mechanistically, c-MET inhibition impaired the reactive mobilization and recruitment of neutrophils into tumors and draining lymph nodes in response to cytotoxic immunotherapies. In the absence of c-MET inhibition, neutrophils recruited to T cell-inflamed microenvironments rapidly acquired immunosuppressive properties, restraining T cell expansion and effector functions. In cancer patients, high serum levels of the c-MET ligand HGF correlated with increasing neutrophil counts and poor responses to checkpoint blockade therapies. Our findings reveal a role for the HGF/c-MET pathway in neutrophil recruitment and function and suggest that c-MET inhibitor co-treatment may improve responses to cancer immunotherapy in settings beyond c-MET-dependent tumors.

INTRODUCTION

Stromal release of hepatocyte growth factor (HGF) and increased expression of its receptor c-MET are found in many solid cancers (Finisguerra et al., 2016). c-MET is a receptor tyrosine kinase encoded by the *MET* proto-oncogene that activates several intracellular signaling pathways including RAS-MAPK, PI3K-AKT, RAC1, and PAK (Graveel et al., 2013). Thereby, c-MET signaling regulates proliferation, cell survival, and migration in development, tissue regeneration, and tumorigenesis. Clinical trials aimed at evaluating the therapeutic benefit of c-MET inhibitors in cancers with deregulated c-MET signaling, either targeting c-MET as a primary oncogenic driver or

preventing c-MET-driven resistance to other oncogenic kinase inhibitors, are currently ongoing (Finisguerra et al., 2016).

c-MET signaling also participates in the regulation of immune responses. Several studies reported immunosuppressive roles for the HGF/c-MET axis such as an impairment of dendritic cell (DC) functions and the induction of T cell tolerance (Benkhoucha et al., 2010; Okunishi et al., 2005). On the other hand, c-MET signaling was shown to promote immunity by driving the emigration of skin-resident DCs to the draining lymph node in a mouse model of contact hypersensitivity (Baek et al., 2012).

Here, we investigated the influence of c-MET inhibition on the efficacy of cancer immunotherapy. We found that c-MET inhibition improved different T cell-directed immunotherapeutic approaches such as adoptive T cell transfer and checkpoint blockade in various solid cancer mouse models, regardless of whether the tumor growth was c-MET dependent or not. Mechanistically, c-MET signaling promoted the reactive recruitment of neutrophils from the bone marrow into lymph node and tumor tissues where they restrained T cell expansion and effector functions. Genetic or pharmacological blockade of c-MET-dependent reactive neutrophil responses promoted T cell infiltration into tumors and thereby improved the efficacy of cancer immunotherapies.

RESULTS

Concomitant c-MET Inhibition Enhances Adoptive T Cell Transfer Immunotherapy

Immunoregulation by c-MET inhibition could result from direct effects on immune cells, on tumor cells, or both. To dissect these possibilities, we used the HCmel12 and B16F1 melanoma cell lines. HCmel12 cells were established from a primary melanoma in *Hgf-Cdk4*^{R24C} mice (Bald et al., 2014a), where transgenic expression of HGF provides constitutive c-MET signaling. Accordingly, growth of HCmel12 cells in culture was inhibited at low nanomolar concentrations by the selective c-MET inhibitor capmatinib (Figure 1A, left; Liu et al., 2011). In contrast, B16F1 melanoma cells proved to be insensitive to capmatinib (Figure 1B, left), in line with previous reports (Shojaei et al., 2010). Next, we established a protocol for capmatinib co-treatment of C57BL/6 mice bearing intracutaneously (i.c.) injected syngeneic HCmel12 or B16F1 melanomas. A 5-day capmatinib monotherapy transiently blocked the growth of established HCmel12 melanomas (Figure 1A, right). We observed no significant change in the growth of B16F1 melanomas treated in the same way (Figure 1B, right). Immunoblots confirmed c-MET on-target activity of capmatinib showing reduced c-MET phosphorylation *in vitro* and *in vivo* in both models (Figures S1A and S1B). However, capmatinib blocked phosphorylation of ERK and AKT only in HCmel12 but not in B16F1 verifying that mitogenic signaling is c-MET dependent only in HCmel12.

To study immunoregulation by c-MET signaling, we first used our previously established adoptive T cell transfer (ACT) protocol (Kohlmeyer et al., 2009; Landsberg et al., 2012). It consists of chemotherapeutic conditioning with a single dose of cyclophosphamide, intravenous injection of CD90.1^{+}CD8^{+} TCR-transgenic Pmel-1 T cells directed against the endogenous melanocytic antigen gp100, activation of T cells *in vivo* with a gp100-expressing adenovirus vaccine, and stimulation of the innate immune system with CpG+poly(I:C). We found that short-term concomitant c-MET inhibition with capmatinib further improved this effective ACT immunotherapy in mice bearing c-MET-dependent HCmel12 melanomas (Figures 1C and S1C). Interestingly, capmatinib also enhanced ACT efficacy in mice bearing c-MET-independent B16F1 melanomas (Figures 1D and S1D). In both models we observed a significantly prolonged survival and more tumor eradications in mice receiving capmatinib together with ACT immunotherapy. Capmatinib co-administration also increased vitiligo-like fur depigmentation in ACT-treated mice with long-term survival (Figures 1E and 1F). Capmatinib co-treatment also improved ACT immunotherapy in our primary *Hgf-Cdk4*^{R24C} melanoma model (Figures S1E and S1F). PF-04217903, a second c-MET inhibitor, showed similar ACT-promoting effects (Figures S1H–S1K). Taken together, these findings demonstrated that pharmacological c-MET inhibition enhanced T cell immunotherapy regardless of the tumor cells' dependence on c-MET signaling, which strongly suggested a microenvironmental or systemic immunoregulatory mechanism.

c-MET Inhibition Increases the Number of Tumor-Infiltrating T Cells

The increased vitiligo-like fur depigmentation in capmatinib co-treated mice indicated an intensified and prolonged systemic activity of adoptively transferred Pmel-1 T cells, because they also target gp100-expressing normal melanocytes in the skin resulting in progressive hair graying. Indeed, we detected increased numbers of Pmel-1 T cells in the blood of mice that received short-term capmatinib co-treatment with the ACT protocol (Figures 2A, 2B, left, S1G, S1K, and S2A). We also observed a significantly increased number of tumor-infiltrating Pmel-1 T cells (Figures 2B, right, and S2B). More detailed flow cytometric analyses revealed an increased proportion of GrzB^{+} Pmel-1 T cells indicating enhanced cytotoxic activity (Figure 2C). We also found a reduced proportion of intratumoral Pmel-1 T cells expressing the T cell exhaustion markers PD-1 and LAG3 (Figures S2C and S2D) or the T cell senescence marker KLRG1 (Figure 2D). Of note, high expression of KLRG1 has been shown to correlate with a reduced proliferative capacity of CD8^{+} T cells in several infectious disease mouse models and humans (Hikono et al., 2007; Sarkar et al., 2008; Voehringer et al., 2002). Thus, the increased number and the phenotype change of tumor-infiltrating Pmel-1 T cells in capmatinib co-treated mice were in concert with an enhanced anti-tumoral activity of the combination treatment.

c-MET Inhibition Impairs the Reactive Recruitment of Tumor-Infiltrating Neutrophils in Response to Immunotherapy

In order to understand how concomitant c-MET inhibition promoted T cell expansion and effector functions, we also searched for changes in other immune cell populations, as these might be involved in the immunoregulation. Interestingly, we observed a reactive increase of CD11b^{+}Ly6G^{+} neutrophils in the peripheral blood within days after ACT therapy that was significantly inhibited by capmatinib (Figures 2E and S2E and Table S1). To investigate how ACT and capmatinib co-treatment affected the number of circulating neutrophils, we analyzed the bone marrow.

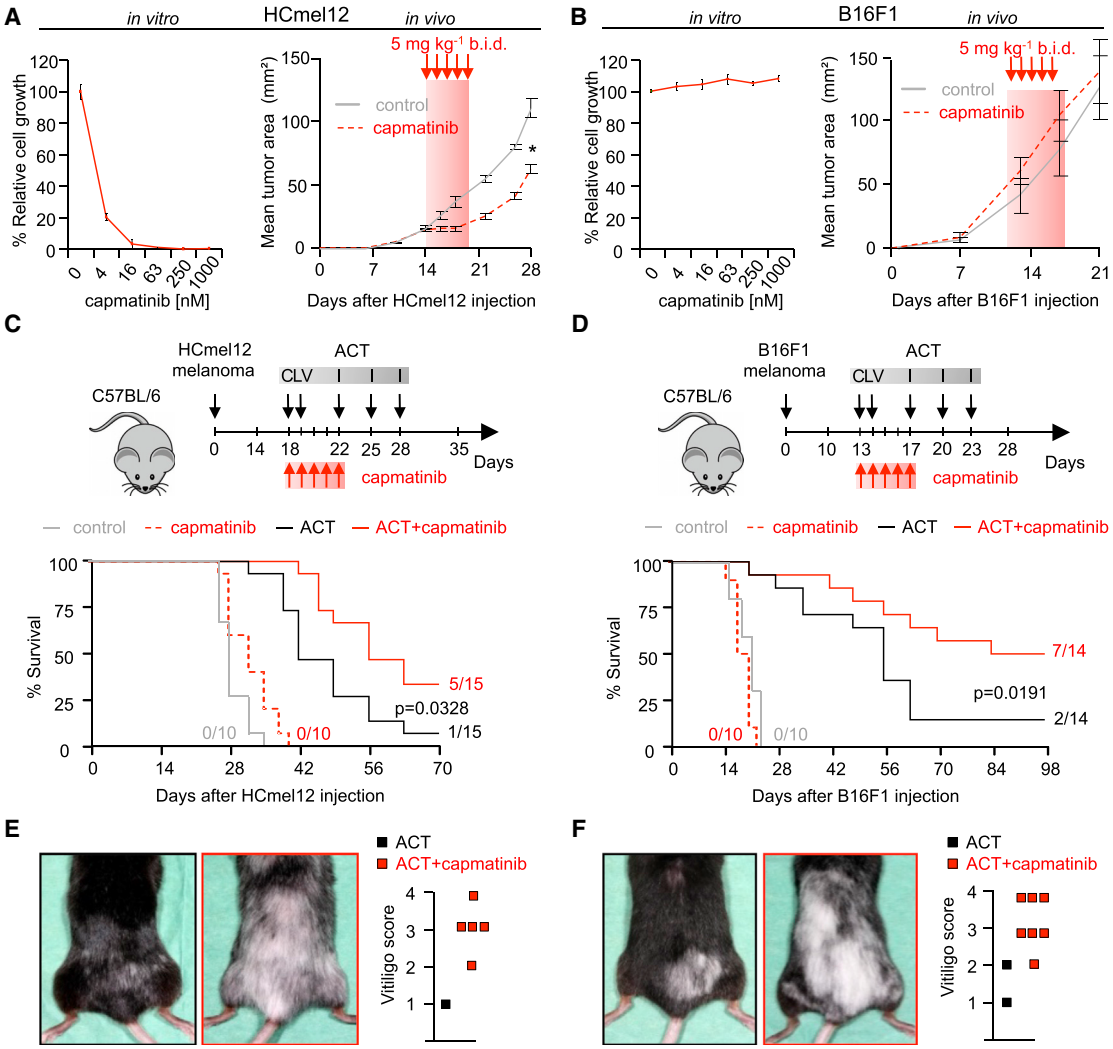

Figure 1. Concomitant Short-Term c-MET Inhibition Enhances the Efficacy of ACT Immunotherapy in Both c-MET-Dependent and c-MET-Independent Melanoma Models

(A and B) Left: Effect of the c-MET inhibitor capmatinib on *in vitro* growth of melanoma cells shown in percent relative to controls (n = 3, mean ± SEM). Right: *In vivo* growth kinetics of tumor transplants treated as indicated (n = 6; mean tumor area ± SEM).

(C and D) Experimental protocols for concomitant capmatinib treatment (5 mg/kg b.i.d.) with ACT immunotherapy (top; C, cyclophosphamide; LV, adenoviral vaccination and Pmel-1 T cell transfer; I, innate immune activation with poly(I:C) and CpG) and Kaplan-Meier survival curves for cohorts of mice treated as indicated (bottom; n = 10 or 15 for HCmel12, n = 10 or 14 for B16F1; numbers behind curves indicate mice with eradicated tumors).

(E and F) Representative pictures of vitiligo-like fur depigmentation on back skin (left) and corresponding quantification (right) in individual long-term surviving mice (n = 6 for HCmel12, n = 9 for B16F1).

Cumulative results of three independent experiments are shown in (C)–(F). Statistics: unpaired two-tailed Student's t test *p < 0.05 (A and B); log rank test for survival curves (C and D). See also Figure S1.

We found an increase of mature neutrophils in bone marrow mononuclear cells (BMMNCs) of ACT-treated mice, showing that this regimen promoted neutrophil mobilization (Figures 2F and 2G). Surprisingly, capmatinib co-treatment resulted in an additional increase of mature neutrophils in the bone marrow with a rise of c-MET-expressing neutrophils from ~2% to ~15% (Figures 2F and 2G). We concluded that c-MET inhibition selectively impaired the reactive egress of neutrophils from the bone marrow into the circulation in response to ACT immunotherapy. These findings agree with the recently described important role of c-MET signaling in neutrophil transendothelial migration (Finisguerra et al., 2015). c-MET signaling has been also shown to enhance bone marrow progenitor expansion (Jalili et al., 2010; Tesio et al., 2011) and we found a reactive increase of granulocytic-macrophage progenitors (GMPs) upon ACT immunotherapy, an effect that was again diminished by capmatinib co-treatment (Figures S2F and S2G). ACT immunotherapy also elicited a reactive influx of c-MET$^+$ neutrophils into tumor tissues, which was again impaired by capmatinib co-treatment (Figure 2H). Thus, c-MET signaling promoted neutrophil mobilization from the bone marrow and their transendothelial migration into inflamed tissues in response to ACT immunotherapy.

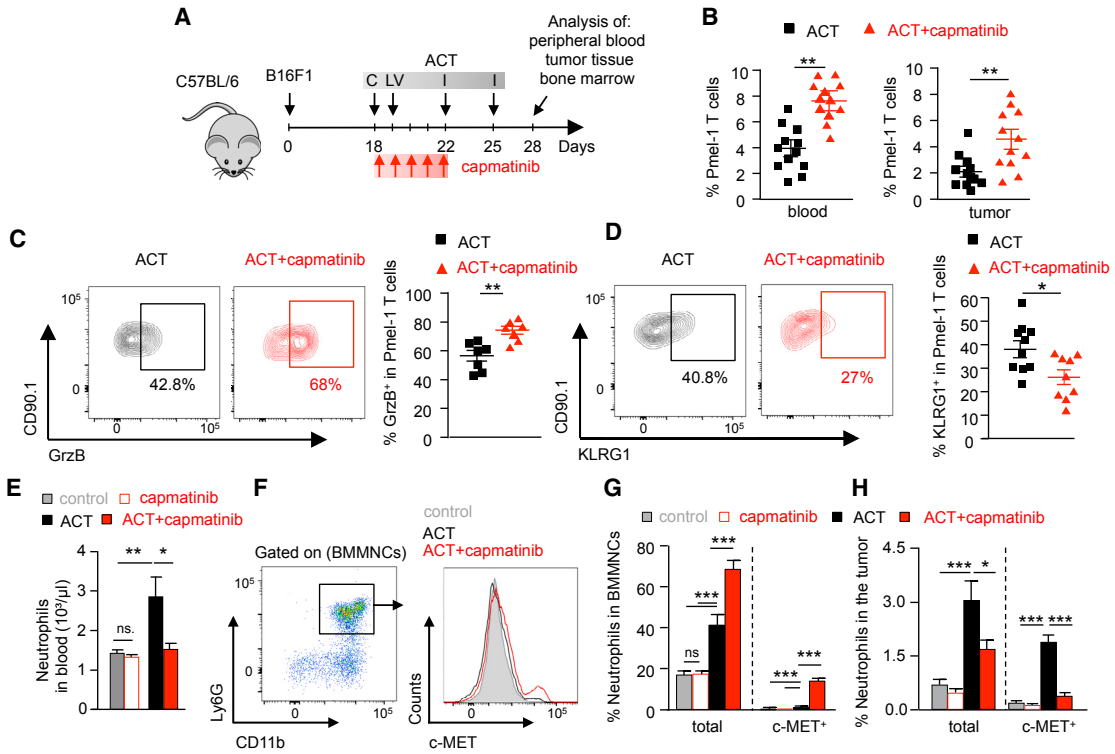

Figure 2. Combining c-MET Inhibition with ACT Immunotherapy Increases the Infiltration of Tumors with Pmel-1 T Cells and Decreases the Reactive Recruitment of c-MET$^+$ Neutrophils

(A) Experimental protocol for the analysis of immune cells in blood, tumors, and bone marrow.

(B) Flow cytometric quantification of Pmel-1 T cells in the blood and tumors of mice treated as indicated (n = 12; mean ± SEM).

(C) Representative flow cytometric plots showing Granzyme B (GrzB) expression on CD90.1$^+$CD8$^+$ Pmel-1 T cells in the tumor (left) and quantification in individual mice treated as indicated (right, n = 7; mean ± SEM).

(D) Corresponding data for KLRG1 (n = 10 for ACT, n = 9 for ACT+capmatinib; mean ± SEM).

(E) Absolute neutrophil counts in the blood of mice on day 22 (for control and capmatinib) or day 28 (for ACT and ACT+capmatinib) treated as indicated (n = 5 for control and capmatinib, n = 12 for ACT and ACT+capmatinib; mean ± SEM).

(F) Gating strategy for c-MET$^+$ neutrophils in BMMNCs.

(G) Quantification of total and c-MET$^+$ neutrophils in BMMNCs of mice treated as indicated (n = 12; mean ± SEM).

(H) Flow cytometric quantification of total and c-MET$^+$ neutrophils in tumors of mice treated as indicated (n = 12; mean ± SEM).

Cumulative results of three independent experiments are shown. Statistics: unpaired two-tailed Student's t test *p < 0.05, **p < 0.01 (E); unpaired two-tailed Mann-Whitney test *p < 0.05, **p < 0.01, and ***p < 0.001 (B–D, G–H). See also Figure S2 and Table S1.

Neutrophils Acquire an Immunosuppressive Phenotype in T Cell Inflamed Microenvironments

We hypothesized that reactive mobilization and recruitment of neutrophils limited the efficacy of ACT immunotherapy, because neutrophils have been shown to acquire T cell-suppressive capacity during tumor progression (Coffelt et al., 2015). Therefore, we investigated the phenotype of neutrophils isolated from different tissues in tumor-bearing mice following ACT immunotherapy by RNA-seq. Neutrophils from tumor tissue and tumor-draining lymph node expressed typical immunosuppressive genes (e.g., *Nos2/iNOS*, *Arg1*, *Cd274/PD-L1*) (Gabrilovich et al., 2012), in contrast to neutrophils isolated from bone marrow, blood, or spleen of the same mice (Figure 3A). Flow cytometric analyses confirmed that more than 85% of neutrophils from tumor tissue and from tumor draining lymph nodes of ACT-treated mice expressed PD-L1 on their surface, in contrast to fewer than 15% of neutrophils from bone marrow or spleen (Figure 3B, top). This confirmed the results of our RNA-seq analysis at the protein level. Most neutrophils from tumor tissue and lymph nodes were also positive for c-MET surface expression (Figure 3B, bottom). Given that PD-L1 is induced by IFN-γ and activated T cells release IFN-γ, we reasoned that neutrophils acquired the immunosuppressive phenotype in response to activated Pmel-1 T cells which encounter their cognate antigen and secrete IFN-γ first in the lymph nodes and then in the tumor. To test this hypothesis, we isolated neutrophils from a non-inflamed tissue (bone marrow) and co-cultured them with gp100 peptide/IL-2-activated Pmel-1 T cells. Neutrophils were able to potently suppress Pmel-1 T cell proliferation and IFN-γ secretion (Figure 3C). In addition, RNA-seq analysis revealed that neutrophils acquired an immunosuppressive phenotype upon exposure to T cell-conditioned medium (Figure 3D) and rapidly upregulated PD-L1 surface expression upon IFN-γ treatment (Figure 3E). Functional analyses with PD-L1 blocking antibodies and neutrophils from iNOS-deficient mice (Laubach et al., 1995) verified that PD-L1 and iNOS, two previously described

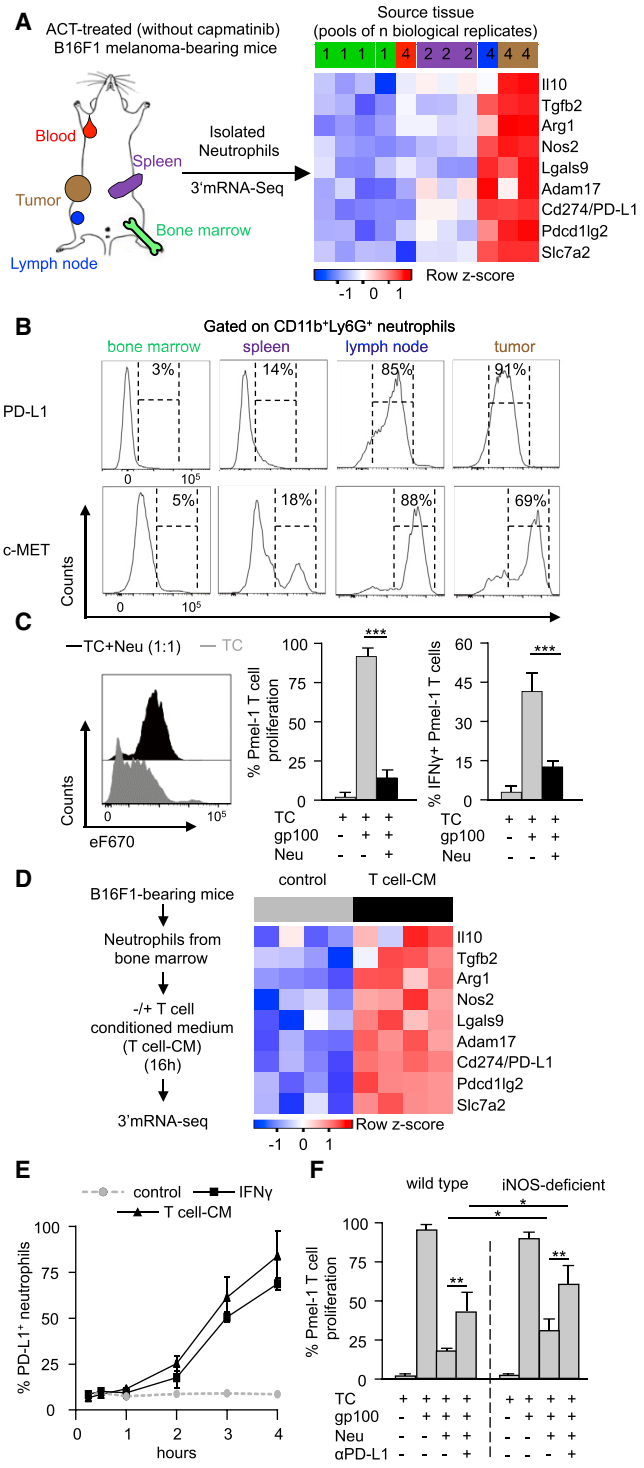

Figure 3. Neutrophils Acquire an Immunosuppressive Phenotype in T Cell-Inflamed Microenvironments of Draining Lymph Node and Tumor Tissues of ACT-Treated Mice

(A) Outline of 3′mRNA-seq analysis comparing neutrophils isolated from different tissues 10 days after T cell transfer (left) and corresponding heatmap visualization (right; numbers in boxes indicate number of pooled biological samples).

(B) Representative flow cytometric plots showing PD-L1 (top) and c-MET (lower) surface staining on CD11b$^+$Ly6G$^+$ neutrophils in indicated organs from ACT-treated mice.

(C) T cell proliferation assay based on eF670 fluorescent dye labeling. Representative flow cytometric plots at indicated conditions (left), cumulative results shown as percent of proliferated Pmel-1 T cells (TC) (middle) and percent of IFN-γ$^+$ Pmel-1 T cells after activation with gp100 peptide and IL-2 and incubation with neutrophils (Neu) isolated from B16F1 melanoma-bearing mice at a ratio 1:1 for 72 hr (right, n = 3; mean ± SEM).

(D) 3′mRNA-seq analysis of neutrophils isolated from the bone marrow stimulated with T cell conditioned medium (T cell-CM) compared to control. Heatmap visualizes z-score transformed log2 rpm (reads per million) gene expression values.

(E) Flow cytometric quantification of PD-L1 expression on bone marrow neutrophils upon IFN-γ or T cell-CM stimulation over time (n = 3; mean ± SEM).

(F) T cell proliferation assay with neutrophils isolated from C57BL/6 or iNOS-deficient B16F1 melanoma-bearing mice at a ratio 1:1 ± αPD-L1 for 72 hr (n = 3; mean ± SEM).

Statistics: unpaired two-tailed Mann-Whitney test *p < 0.05, **p < 0.01, and ***p < 0.001 (C–F).

immunosuppressive mechanisms by neutrophils (Bowers et al., 2014; Coffelt et al., 2015; Gabrilovich et al., 2012), impaired T cell proliferation in an additive manner (Figure 3F). These *ex vivo* assays showed that induction of immunosuppressive genes and T cell-suppressive properties in neutrophils were directly linked to the presence of activated T cells releasing IFN-γ and other cytokines.

c-MET Inhibition Promotes T Cell Expansion in the Tumor-Draining Lymph Node by Impairing Reactive Neutrophil Recruitment

We were intrigued by our finding that neutrophils were recruited to lymph nodes during ACT immunotherapy (Figures 3A and 3B). Neutrophils are usually rare in lymph nodes under non-inflammatory conditions but they can be recruited during acute infections and participate in immunoregulation (Chtanova et al., 2008; Hampton et al., 2015; Kastenmüller et al., 2012; Yang and Unanue, 2013; Yang et al., 2010). Using flow cytometric analyses and a fluorescent reporter mouse model specific for neutrophils (Hasenberg et al., 2015), we demonstrated that c-MET$^+$ neutrophils infiltrated the tumor draining lymph nodes in response to ACT immunotherapy. In line with our findings shown so far, this was diminished by capmatinib co-treatment (Figures 4A, 4B, and S3A). Importantly, impaired recruitment of neutrophils was associated with a reciprocal increase of Pmel-1 T cell numbers in the tumor-draining lymph nodes (Figure 4C, left). Furthermore, a higher fraction of Pmel-1 T cells expressed the proliferation marker Ki67$^+$, which suggested a more effective activation and could also explain their increased systemic expansion observed in mice co-treated with capmatinib (Figure 4C, right). Using fluorescent reporter mice (Figure 4D), analyses of 3D fluorescent images indicated close associations between tdTomato$^+$ neutrophils and GFP$^+$ Pmel-1 T cells in lymph nodes (Figure 4E). Automated distance analysis revealed that about half of tdTomato$^+$ neutrophils were closer than 20 μm to GFP$^+$ Pmel-1 T cells (Figures S3B–S3D). Previously, we established these distance parameters as a relevant measure for functional CD8$^+$ T cell interactions with antigen-presenting cells within the lymph node (Eickhoff et al., 2015). Furthermore, two-photon intravital microscopy provided evidence for direct physical interactions between neutrophils and Pmel-1 T cells in lymph nodes that lasted for several minutes (Figure S3E). Altogether, these

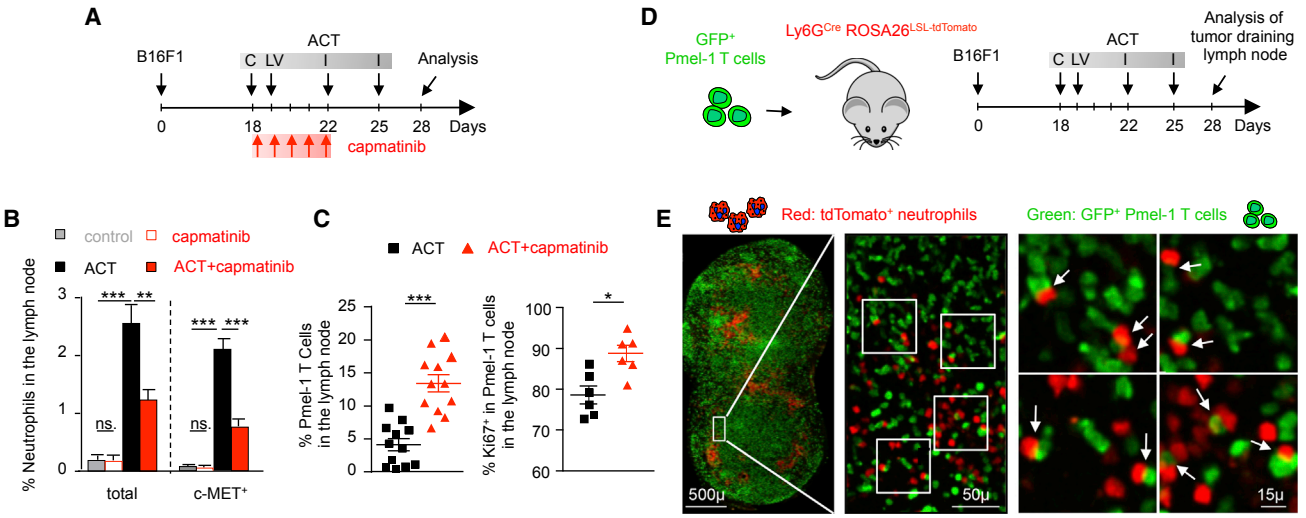

Figure 4. c-MET Inhibition Decreases the Reactive Recruitment of c-MET$^+$ Immunosuppressive Neutrophils in Lymph Node Tissues and Promotes Pmel-1 T Cell Expansion

(A) Experimental protocol for the analysis of neutrophils and Pmel-1 T cells in the B16F1 melanoma model.

(B) Flow cytometric quantification of total and c-MET$^+$ neutrophils in the tumor draining lymph node of mice treated as indicated (right; n = 12; mean ± SEM).

(C) Flow cytometric quantification of Pmel-1 T cells (left, n = 12; mean ± SEM) and of Ki67$^+$ expression in Pmel-1 T cells (right, n = 6; mean ± SEM) in the tumor draining lymph node of mice treated as indicated.

(D) Experimental protocol for the analyses of neutrophils in tumor draining lymph nodes of Ly6G^{Cre}ROSA26$^{LSL\text{-}tdTomato}$ mice treated with ACT immunotherapy.

(E) Representative fluorescent images showing the localization of tdTomato$^+$ neutrophils and adoptively transferred GFP$^+$ Pmel-1 T cells in the tumor draining lymph node on day 10 after ACT immunotherapy. White arrows indicate interaction between neutrophils and Pmel-1 T cells.

Cumulative results of three independent experiments are shown. Statistics: unpaired two-tailed Mann-Whitney test *p < 0.05, **p < 0.01, ***p < 0.001 (B and C). See also Figures S3 and S4.

findings substantiated the notion that c-MET-dependent reactive neutrophil infiltration into lymph nodes restrained anti-tumor T cell expansion, likely through direct interactions as well as indirect mechanisms within a shared microenvironment.

Genetic Ablation of c-MET Kinase Activity Specifically in Neutrophils Enhances ACT Immunotherapy

To corroborate whether c-MET inhibition in neutrophils was indeed critical, we used the previously described mouse model (Finisguerra et al., 2015; Huh et al., 2004), where c-MET kinase activity is ablated by Cre-mediated conditional deletion of exon 16 encoding for the cytoplasmic ATP-binding pocket specifically in neutrophils (*Met*$^{exon16\Delta Neu}$ mice). ACT immunotherapy of established B16F1 melanomas was significantly more effective in *Met*$^{exon16\Delta Neu}$ mice than in littermate controls (Figures S4A–S4C). Furthermore, *Met*$^{exon16\Delta Neu}$ mice showed extensive vitiligo-like fur depigmentation (Figure S4D) and increased Pmel-1 T cell numbers in the blood, tumor, and draining lymph node (Figure S4E). Again, this was linked to a diminished reactive systemic neutrophil response (Figure S4F) through selective retention of neutrophils in the bone marrow (Figure S4G). As the N-terminal part of the kinase-inactive c-MET receptor is still expressed and detectable by flow cytometry on the surface of neutrophils from *Met*$^{exon16\Delta Neu}$ mice, the accumulation of c-MET$^+$ neutrophils in ACT-treated *Met*$^{exon16\Delta Neu}$ mice corroborated that c-MET kinase activity was critically required for the reactive neutrophil egress from the bone marrow. Reactive neutrophil infiltration of tumor and tumor-draining lymph node was also impaired in *Met*$^{exon16\Delta Neu}$ mice undergoing ACT immunotherapy (Figure S4H). In conclusion, the genetic ablation of c-MET signaling specifically in neutrophils in the *Met*$^{exon16\Delta Neu}$ model recapitulated the immunoregulatory effects of pharmacological c-MET blockade. These results provided strong evidence that c-MET inhibitors enhanced ACT immunotherapy largely due to inhibition of c-MET signaling in neutrophils.

Concomitant c-MET Inhibition Enhances the Efficacy of Checkpoint Blockade Immunotherapy

Next, we asked whether concomitant c-MET inhibition could also improve other types of cancer immunotherapy. We treated mice bearing established B16F1 melanomas with a combination of anti-PD-1 antibody and poly(I:C)+CpG (i.e., PCP regimen) and found that concomitant c-MET inhibition also improved this treatment approach (Figures 5A and S5A). Peritumoral injection of poly(I:C)+CpG is commonly used to activate the innate immune system in order to enforce immune responses in T cell-poor tumors like B16F1, because PD-1 blockade would be otherwise ineffective (Bald et al., 2014b; Nagato et al., 2014). We obtained similar results when treating mice bearing established LLC lung cancers (s.c.) with the PCP regimen (Figures 5B and S5B). We also used the MC38 colon cancer model, because it is more immunogenic and responsive to systemic anti-PD-1 monotherapy (Ngiow et al., 2015). c-MET inhibition with capmatinib was also effective in this experimental setting (Figures 5C and S5C). Lastly, capmatinib co-administration also improved the treatment of 4T1.2 mammary tumors orthotopically transplanted into the mammary fat pads of BALB/c mice with anti-PD-1 blocking and anti-CD137 agonistic

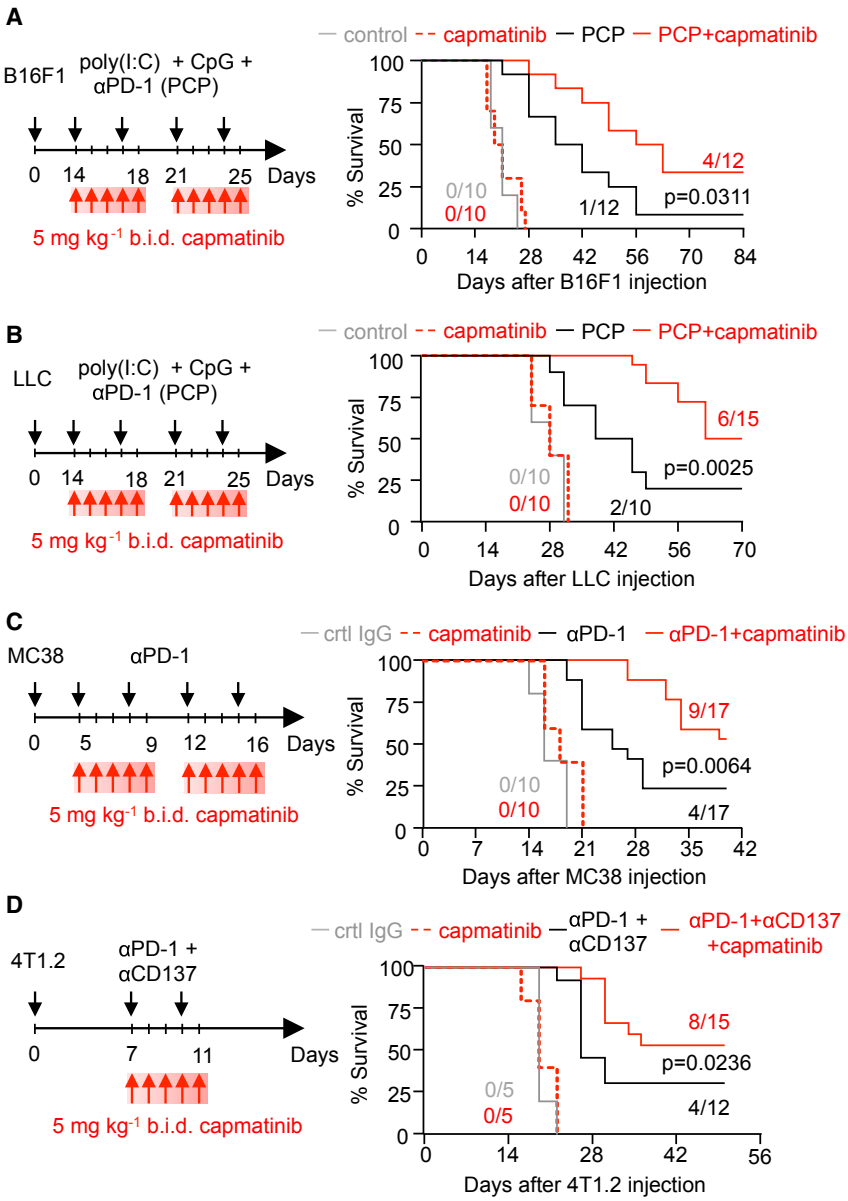

Figure 5. Concomitant Short-Term c-MET Inhibition Enhances the Efficacy of Checkpoint Blockade Immunotherapy across Different c-MET-Independent Tumor Models

(A) Experimental protocol for concomitant capmatinib treatment with PCP immunotherapy (poly(I:C) + CpG + αPD-1) in the B16F1 melanoma model (left) and Kaplan-Meier survival curves (right) for cohorts of mice treated as indicated (n = 10 for control and capmatinib, n = 12 for PCP and PCP+capmatinib; numbers indicate mice with eradicated tumors).

(B) Corresponding data in the LLC lung cancer model (n = 10 for control, capmatinib and PCP, n = 15 for PCP+capmatinib).

(C) Corresponding data for concomitant capmatinib treatment with αPD-1 immunotherapy in the MC38 colon cancer model (n = 10 for control and capmatinib, n = 17 for αPD-1 and αPD-1+capmatinib).

(D) Corresponding data for concomitant capmatinib treatment with αPD-1+αCD137 immunotherapy in the 4T1.2 mammary cancer model (n = 5 for control and capmatinib, n = 12 for αPD-1+αCD137, n = 15 for αPD-1+αCD137+capmatinib).

Cumulative results of three independent experiments are shown. Statistics: log-rank test. See also Figure S5.

antibodies (Figures 5D and S5D). Of note, all four tumor models used were insensitive to capmatinib *in vitro* and short-term capmatinib treatment alone had no effect on tumor growth *in vivo* (Figures 5A–5D, S5E, 1D, and S1D). Hence, c-MET inhibition synergistically improved different types of immunotherapies in various solid cancer models regardless of the tumor cell's dependence on c-MET signaling. These results further corroborated the immunoregulatory capacity of concomitant c-MET inhibition.

Concomitant c-MET Inhibition Reinforces Antigen-Specific CD8$^+$ T Cell Responses during Immune Checkpoint Therapy

Flow cytometric analyses demonstrated that capmatinib co-treatment increased the number of CD8$^+$ T cells in tumor tissues and regional lymph nodes following immunotherapy in the B16, LLC, and MC38 mouse cancer models (Figures S6A–S6I). In mice bearing 4T1.2 mammary cancers, we monitored the spontaneous antigen-specific CD8$^+$ T cell response directed against a defined peptide epitope in gp70 derived from the murine leukemia virus (MLV) by tetramer staining and flow cytometry (Figure 6A; Liu et al., 2016). Capmatinib co-administration in conjunction with anti-PD-1+anti-CD137 immunotherapy significantly increased the frequency of gp70-specific CD8$^+$ T cells in tumors and lymph nodes (Figures 6B and 6C). Importantly, the different immunotherapeutic interventions also consistently elicited reactive recruitment of c-MET$^+$ neutrophils into tumor tissues and regional lymph nodes, an effect that was significantly diminished by capmatinib co-administration (Figures 6D, 6E, and S6A–S6I). Furthermore, the proportion of gp70-specific KLRG1$^+$CD8$^+$ T cells decreased, whereas the proportion of gp70-specific GrzB$^+$CD8$^+$ T cells increased in tumors of capmatinib co-treated mice, in line with improved effector functions (Figures 6F and 6G). In the tumor draining lymph node we also observed a decreased proportion of gp70-specific KLRG1$^+$CD8$^+$ T cells associated with an increased proportion of gp70-specific Ki67$^+$CD8$^+$ T cells in concert with an enhanced expansion (Figures 6H and 6I). These phenotype changes of CD8$^+$ T cells in tumors and lymph nodes were also confirmed in mice bearing MC38 tumors receiving capmatinib in conjunction with anti-PD-1 immunotherapy (Figures S6J and S6K). Taken together, our data support the notion that concomitant c-MET inhibition impaired reactive neutrophil recruitment in response to immune checkpoint therapy which in

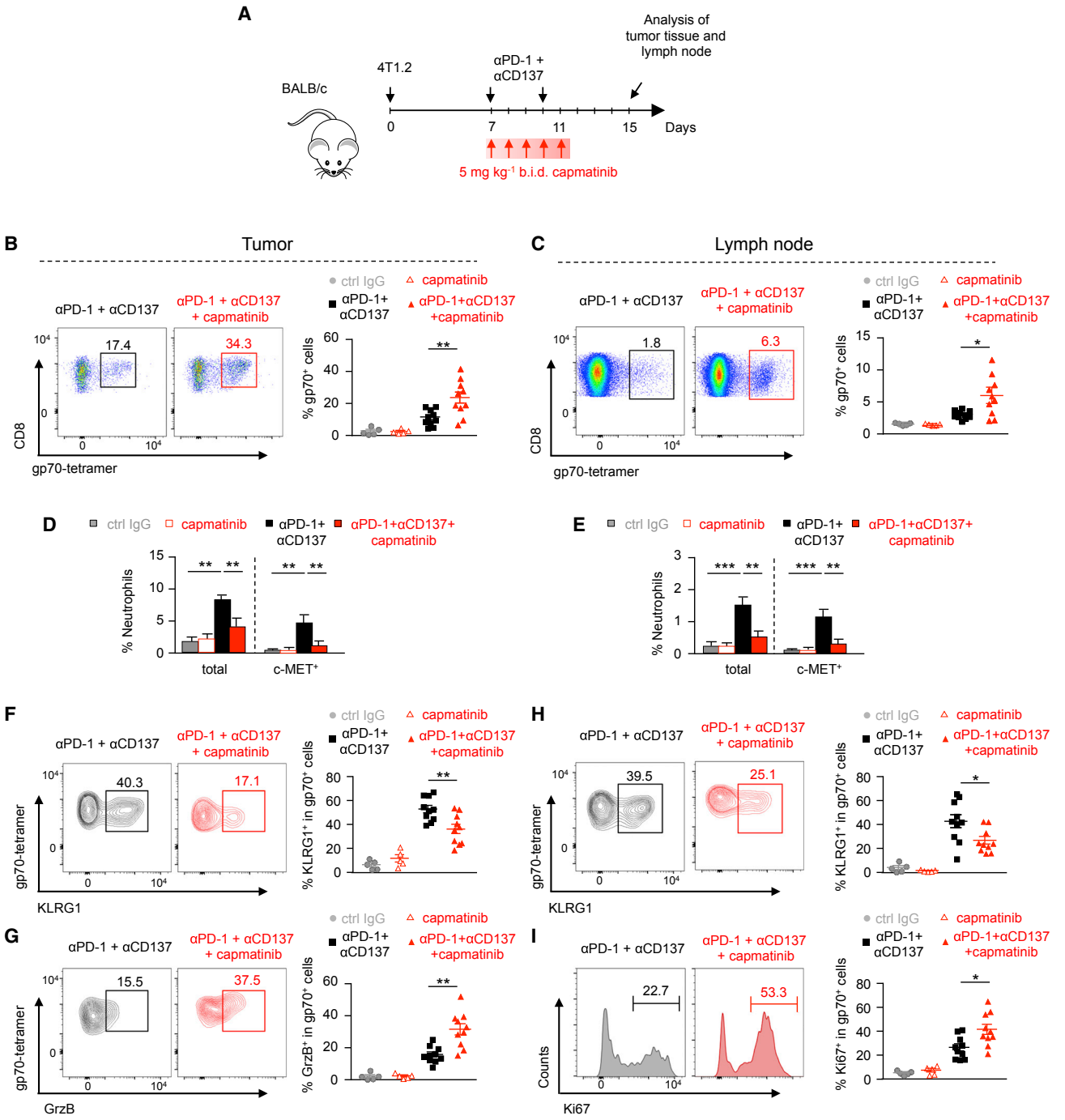

Figure 6. Combining c-MET Inhibition with Checkpoint Blockade Immunotherapy Promotes Effective T Cell Immunity and Impairs Reactive Neutrophil Responses

(A) Experimental protocol for the analysis of immune cells in the 4T1.2 mammary cancer model.

(B and C) Representative flow cytometric plots showing gp70 tetramer$^+$ CD8$^+$ T cells in tumors and draining lymph nodes (left) and quantification (right).

(D and E) Quantification of total and c-MET$^+$ neutrophils in tumors and draining lymph nodes.

(F and G) Expression of KLRG1$^+$ and GrzB$^+$ on gp70 tetramer$^+$ CD8$^+$ T cells in tumors (left) and quantification (right).

(H and I) Expression of KLRG1$^+$ and Ki67$^+$ on gp70 tetramer$^+$ CD8$^+$ T cells p70$^+$ T cells in draining lymph nodes (left) and quantification (right).

In all experiments n = 5 for control and capmatinib, n = 10 for αPD-1+αCD137 and αPD-1+αCD137+capmatinib (mean ± SEM). Statistics: unpaired two-tailed Mann-Whitney test; *$p < 0.05$, **$p < 0.01$, and ***$p < 0.001$ (B–I). See also Figure S6.

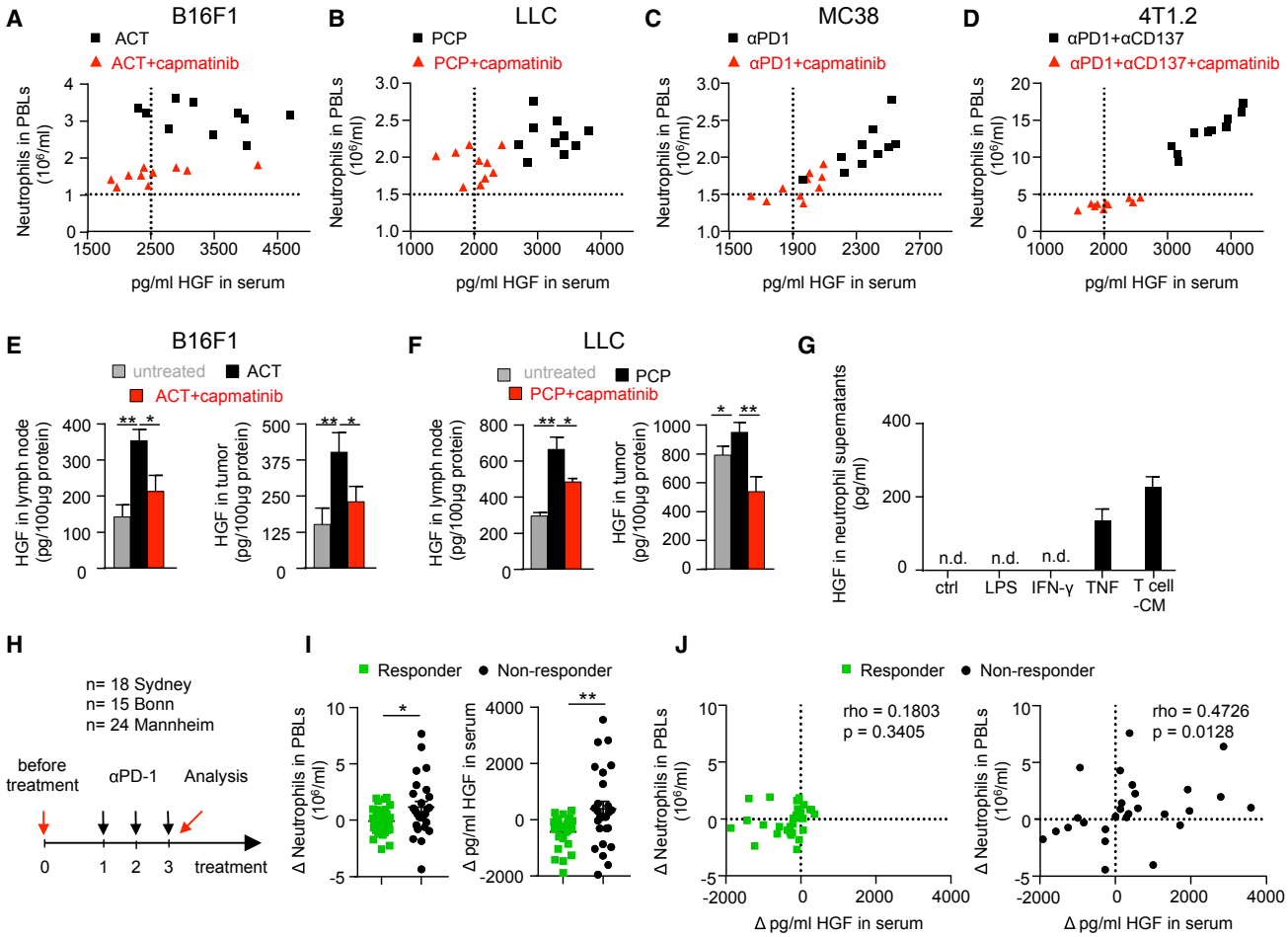

Figure 7. Increases of Serum HGF and Neutrophil Counts Correlate with Unresponsiveness to Anti-PD-1 Immunotherapy in a Subgroup of Patients with Metastatic Melanoma

(A–D) Scatterplot showing absolute neutrophil counts in peripheral blood leukocytes (PBLs) versus HGF serum levels of individual mice bearing B16F1 (A), LLC (B), MC38 (C), and 4T1.2 (D) tumors on day 7–10 after start of indicated therapy (n = 10 for each cohort).

(E) HGF levels per 100 µg protein in lymph node and melanoma tissues of B16F1 melanoma-bearing mice 10 days after start of indicated therapy (n = 12; mean ± SEM).

(F) Corresponding data for LLC tumor-bearing mice 7 days after start of indicated therapy (n = 12; mean ± SEM).

(G) HGF levels in supernatants of bone marrow neutrophils isolated from B16F1 melanoma-bearing mice stimulated with indicated conditions for 18 hr (n = 3; mean ± SEM).

(H) Blood samples from 57 melanoma patients before and after 3 doses of αPD-1 immunotherapy from 3 different clinical centers have been assessed for neutrophil counts and serum HGF levels.

(I) Changes in measurements of absolute neutrophil counts in PBLs (left) and HGF serum levels (right) before treatment onset and after the third treatment (n = 30 responder, n = 27 non-responder; mean ± SEM).

(J) Corresponding scatterplot showing changes in absolute neutrophil counts in PBLs versus changes in HGF serum levels (n = 30 for responder; n = 27 for non-responder). Correlation between neutrophil counts and HGF levels determined by Spearman's rank correlation (rho).

Statistics: unpaired two-tailed Student's t test *p < 0.05; **p < 0.01 (E and F); unpaired two-tailed Mann-Whitney test *p < 0.05; **p < 0.01 (I); Spearman's rank correlation test (J). See also Figure S7 and Table S2.

turn allowed for increased expansion and improved effector functions of tumor antigen-specific CD8$^+$ T cells resulting in significantly prolonged survival.

Reactive Neutrophil Responses Drive Systemically Increased HGF Levels

All cancer immunotherapy strategies that we investigated in our mouse models evoked reactive increases of blood neutrophil counts, which were decreased by c-MET inhibition with capmatinib co-treatment. Across all models we also observed reactive increases of serum HGF levels, which were again inhibited by capmatinib (Figures S7A–S7E, left). On treatment, HGF levels correlated with blood neutrophil counts and separated samples from mice that received concomitant capmatinib from those that were treated with immunotherapy only (Figures 7A–7D). We also observed increased HGF levels in lymph node and tumor tissues in ACT-treated mice, which were again diminished by capmatinib co-treatment (Figures 7E and 7F). Thus, these tissues could

be sources of elevated serum HGF levels in response to immunotherapy. In line with published observations (Grenier et al., 2002), we found that TNF and T cell-conditioned medium caused HGF release from isolated mouse neutrophils (Figure 7G). This suggested that HGF release by neutrophils in a T cell-inflamed tumor microenvironment contributes to c-MET-dependent neutrophil recruitment as a feed-forward mechanism. Of note, capmatinib also lowered the ratios between neutrophils and T cells in peripheral blood (Figures S7A–S7E, right). Considering the different treatment outcomes, our results show that increasing blood neutrophil counts, increasing serum HGF levels, and increasing neutrophil-to-T cell ratios correlated with poor responses, whereas stable values correlated with good responses to immunotherapy in our mouse models. Correlations between mRNA expression levels of *HGF* and neutrophil marker genes in human tumors further supported direct links between the HGF/c-MET axis and neutrophils (Figure S7F).

Increasing Blood Neutrophil Counts Are Associated with Increasing Serum HGF Levels in a Subgroup of Melanoma Patients that Poorly Respond to Checkpoint Immunotherapy

It is well known that high blood neutrophil counts and high neutrophil-to-lymphocyte ratios in patients with advanced cancer generally correlate with a poor prognosis (Shen et al., 2014; Templeton et al., 2014). In patients with advanced melanoma, these parameters are specifically associated with a poor response to checkpoint blockade immunotherapy (Ferrucci et al., 2015; Gebhardt et al., 2015). We therefore asked whether increasing blood neutrophil counts and a poor prognosis are also associated with increasing serum HGF levels in the clinical situation, assuming that these parameters show much more variability in patients. For this purpose, we retrospectively determined the change of blood neutrophil counts and serum HGF levels in patients with metastatic melanoma undergoing anti-PD-1 immunotherapy at three independent clinical centers by comparing measurements of pre- and on-treatment samples (Figure 7H and Table S2). We found increases of serum HGF levels along with blood neutrophil counts in a subset of non-responders, but only to a lesser extent in patients responding to anti-PD-1 therapy (Figures 7I and 7J). Even though larger and independent patient cohorts are needed to confirm this, these observations mirror our data obtained in mouse models and are compatible with the notion that the HGF/c-MET signaling axis might also drive reactive neutrophil mobilization in a feed-forward manner and thereby limit the efficacy of cancer immunotherapies in patients with advanced cancer. Our results provide a scientific basis to further investigate this hypothesis in future clinical trials.

DISCUSSION

In our work we demonstrated that a short course of c-MET inhibitor co-treatment increased the efficacy of adoptive T cell and checkpoint immunotherapy strategies in several widely studied mouse tumor models. Importantly, this therapeutic effect was observed even in the absence of tumor cell-intrinsic c-MET dependence. c-MET inhibition also enhanced adoptive T cell immunotherapy of primary autochthonous melanomas in a genetically engineered mouse model, further supporting the generality of our observations. c-MET inhibition in combination with immunotherapy further increased the absolute numbers and enhanced the effector functions of antigen-specific $CD8^+$ T cells in tumor tissues. Interestingly, we discovered that c-MET inhibition substantially modulated the phenotype of tumor-infiltrating $CD8^+$ T cells. An increased proportion of $CD8^+$ T cells expressed GrzB whereas a reduced proportion expressed KLRG1. This consistently correlated with enhanced anti-tumor T cell responses across different mouse tumor models. Of note, KLRG1 is considered as a $CD8^+$ T cell senescence marker and indicates reduced proliferative capacity (Voehringer et al., 2002). Moreover, $KLRG1^+$ effector $CD8^+$ T cells have a reduced likelihood to enter the memory $CD8^+$ T cell state (Sarkar et al., 2008), and $KLRG1^+$ memory $CD8^+$ T cells show reduced expansion after re-stimulation by their cognate antigen (Hikono et al., 2007). Therefore, KLRG1 might represent an important biomarker for effective anti-tumor $CD8^+$ T cell responses that needs to be considered in future studies.

Mechanistically, our experiments in $Met^{exon16\Delta Neu}$ mice where c-MET signaling is genetically blocked specifically in neutrophils provided strong evidence that the immunoregulatory effect of pharmacologic c-MET signaling blockade with capmatinib is largely due to a direct effect on neutrophils. We concluded that c-MET signaling in neutrophils promoted their reactive mobilization from the bone marrow and their subsequent recruitment into tumor tissue and draining lymph nodes in response to cytotoxic immunotherapies. In T cell-inflamed tissues, neutrophils rapidly acquired an immunosuppressive phenotype. This was at least in part mediated through IFN-γ, which is secreted into the shared environment by activated T cells. Our results support recent findings that IFN signaling, though critical for adaptive immunity, also activates multiple immunosuppressive pathways limiting checkpoint immunotherapy (Benci et al., 2016). We implicate c-MET signaling as a critical driver of a neutrophil-mediated resistance program to cancer immunotherapy.

Our observations touch upon the controversial and Janus-faced role of neutrophils, which can exert both anti- and pro-tumoral activities depending on the context. This was already observed decades ago (Gerrard et al., 1981; Pekarek et al., 1995). More recent studies defined molecular and cellular mechanisms of anti-tumoral (Blaisdell et al., 2015; Eruslanov et al., 2014; Finisguerra et al., 2015; Granot et al., 2011; Singhal et al., 2016) as well as pro-tumoral (Bald et al., 2014a; Coffelt et al., 2015; Fridlender et al., 2009; Mishalian et al., 2013; Wculek and Malanchi, 2015) effects of neutrophils in different experimental settings. Our results shed further light on the highly context-dependent regulation of neutrophil functions and support the emerging notion that neutrophils have anti-tumoral properties early during tumor development and acquire pro-tumoral features in progressively growing tumors and in response to immunotherapeutic intervention, as shown in our work. This highlights the extraordinary plasticity of neutrophils, which is increasingly appreciated as a critical driver of their functional diversity (Nicolás-Ávila et al., 2017; Sagiv et al., 2015).

Our data also substantiate the emerging immunoregulatory functions of neutrophils in lymph nodes, which have been addressed so far largely in the context of immunization and infection (Chtanova et al., 2008; Hampton et al., 2015;

Kastenmüller et al., 2012; Yang and Unanue, 2013). Reactive neutrophil recruitment to lymph nodes was shown to limit cellular and humoral immune responses to vaccination antigens and pathogens (Kamenyeva et al., 2015; Yang et al., 2010). We show that different types of immunotherapies can drive reactive c-MET-dependent neutrophil recruitment into tumor-draining lymph nodes, which restrains the expansion of anti-tumoral $CD8^+$ T cells. As recently also appreciated by others (Spitzer et al., 2017), our finding underscores the importance of systemic immunity coordinated in secondary lymphoid organs to sustain an effective anti-tumor T cell response.

Because the HGF/c-MET signaling axis regulates physiological and pathophysiological tissue regeneration (Trusolino et al., 2010), we propose that activation of this pathway occurs as a wounding-like response to cancer immunotherapy (Hölzel et al., 2013). Infiltration of activated immune cells may release HGF, which is normally sequestered at extracellular matrix components (Hattori et al., 2004). Furthermore, inflammation and other stress conditions like hypoxia have been described to activate c-MET signaling (Finisguerra et al., 2015; Pennacchietti et al., 2003). Neutrophils themselves may contribute to this, because they also release HGF, fuel inflammation, and locally deplete oxygen upon transmigration (Campbell et al., 2014; Grenier et al., 2002; Henry et al., 2016). Along this line we found that neutrophils release HGF in response to TNF and T cell-conditioned medium, which suggested that neutrophils could promote their own recruitment into T cell-inflamed environments through HGF release. This explains, at least in part, the increased serum HGF levels observed in all our mouse cancer models undergoing immunotherapy. Our results suggest that HGF links local tissue damage evoked by cancer immunotherapy with a systemic c-MET-dependent neutrophil response that limits therapeutic efficacy.

In support of this concept, HGF cooperates with G-CSF (granulocyte-colony stimulating factor) to promote hematopoietic progenitor cell expansion (Jalili et al., 2010; Tesio et al., 2011). In agreement, we observed that immunotherapies caused myeloid progenitor expansion and neutrophil mobilization from the bone marrow. We uncovered that c-MET signaling was particularly critical for the egress of a subset of ($c\text{-}MET^+$) neutrophils from the bone marrow into the blood in mice undergoing immunotherapy, which is in line with c-MET being implicated in neutrophil transendothelial migration (Finisguerra et al., 2015). The reactive neutrophil response to cancer immunotherapy is reminiscent of the emergency granulopoiesis under infectious conditions (Manz and Boettcher, 2014), but the underlying tumor burden is likely to impose additional changes on neutrophil phenotypes as shown in tumor mouse models of disease progression and advanced stage cancer patients (Coffelt et al., 2015; Sagiv et al., 2015).

High blood neutrophil counts and neutrophil-to-lymphocyte ratios predict poor survival in cancer patients (Shen et al., 2014; Templeton et al., 2014) and poor outcome to checkpoint immunotherapy in melanoma patients (Ferrucci et al., 2015; Gebhardt et al., 2015). Therefore, inhibiting reactive neutrophils emerges as a strategy to enhance cancer immunotherapies. In this respect, concomitant c-MET inhibition is a promising approach, because it impairs a relevant subset of neutrophils at critical tissue sites without blocking or ablating neutrophils in total and thereby increasing the susceptibility for infections. On a more general note, our data emphasize the importance of understanding how oncogenic kinase inhibitors influence immune cell functions, a knowledge that is critical to exploit therapeutic synergism or to predict interference (Crompton et al., 2015; Ebert et al., 2016). Our finding that concomitant c-MET inhibition enhanced different immunotherapies in mouse models for solid cancer provides a scientific basis for further clinical investigation. Currently, c-MET inhibitors are evaluated in clinical trials based on the rationale to target oncogenic c-MET signaling in tumor cells. Exploiting the immunoregulatory capacity of c-MET inhibitors, as demonstrated in our study, could broaden their clinical applicability in combination with cancer immunotherapies.

STAR★METHODS

Detailed methods are provided in the online version of this paper and include the following:

- KEY RESOURCES TABLE
- CONTACT FOR REAGENT AND RESOURCE SHARING
- EXPERIMENTAL MODEL AND SUBJECT DETAILS
  - Mice
  - Cell lines
  - Primary cell cultures
  - Human blood and serum samples
- METHOD DETAILS
  - Cell growth assays
  - Immunoblots
  - Tumor transplantation experiments
  - Induction of Primary Melanomas
  - c-MET inhibition *in vivo*
  - Adoptive cell transfer (ACT) immunotherapy
  - Immunotherapies
  - Vitiligo scoring
  - Tissue digestion
  - Flow cytometry
  - Analysis of absolute immune cell counts
  - Bone marrow analysis
  - Isolation of neutrophils
  - T cell conditioned medium (T cell-CM)
  - 3′mRNA-Seq analysis of neutrophils
  - T cell proliferation and IFN-γ production assay
  - PD-L1 upregulation on neutrophils *in vitro*
  - ELISA
  - Immunofluorescence staining of lymph nodes
  - Quantitative analysis of imaging data
  - Intravital two-photon imaging
  - TCGA transcriptomic analysis
- QUANTIFICATION AND STATISTICAL ANALYSIS
  - Statistical analyses
  - Selection of statistical tests
- DATA AND SOFTWARE AVAILABILITY

SUPPLEMENTAL INFORMATION

Supplemental Information includes seven figures and two tables and can be found with this article online at https://doi.org/10.1016/j.immuni.2017.09.012.

AUTHOR CONTRIBUTIONS

Conceptualization, N.G., T.B., M.M., M.J.S., T.T., M.H.; Methodology, N.G., T.B., S.E.; Software, M.H.; Validation, N.G., T.B., M.M., K.N.; Formal Analysis, N.G., T.B., M.H., S.E., W.K.; Investigation, N.G., T.B., D.vdB.-K., D.H., K.N., J.S.O'D., I.D., S.S., M.B., S.E., W.K., N.S., M.R., J.J.R., T.C.vdS.; Resources, C.W., K.U.L., M.R.-B., A.J.M., J.L., C.G., G.V.L., R.A.S., W.K., M.M., M.J.S., T.T., M.H.; Data Curation, N.G., T.B., M.H.; Writing – Original Draft, N.G., T.B., T.T., M.H.; Writing – Review & Editing, N.G., T.B., W.K., M.M., M.J.S., T.T., M.H.; Supervision, N.G., T.B., W.K., V.J., M.M., E.G., M.W.L.T., M.J.S, T.T., M.H.; Project Administration, T.T., M.H.; Funding Acquisition, C.G., K.U.L., K.N., M.W.L.T., M.R.-B., A.J.M., T.B., M.M., M.J.S., T.T., M.H.

ACKNOWLEDGMENTS

We thank S. Bald, P. Aymans, K. Elder, and L. Town for managing the mouse colonies, K. Keppler and S. Sivalingam for help with NGS, and E. Endel, P. Wurst and An. Dolf for help with FACS sorting. We thank the UKB FACS core facility. We thank the UKB and Mannheim/DKFZ Biobank core facilities. Instruments at the UKB NGS core facility were supported in part by grant DFG-INST 217/674-1 FUGG. T.B. was funded by an EMBO long-term Fellowship (ALT945-2015) and a National Health and Medical Research Council of Australia (NH&MRC) Early Career Fellowship (1124690). K.U.L. was supported by DFG (1944/3-1). M.M. was supported by an ERC starting grant (OxyMO, 308459). M.J.S. was supported by a NH&MRC Research Fellowship (1078671) and M.J.S., K.N, and M.W.L.T. were supported by a NH&MRC Project Grant (1098960). J.S.O'D. was supported by an Australian Post-Graduate Award and QIMR Berghofer PhD Top-Up Scholarship. M.R.-B. and A.J.M. were supported by grants from the DFG (Z01 in the SFB854, MU 3742/2-1). C.G. was supported by a grant from the DFG (GE 2152/2-1). T.T. was funded in part by grants from the DFG (TU 90/8-1, A22 in the SFB704, and A27 in the SFB854). M.H. was funded in part by DFG (HO4281/2-1) and DFG Cluster of Excellence ImmunoSensation (EXC 1023). T.T. and M.H. were funded by Else-Kröner-Fresenius-Stiftung (EKFS 2013_A297). C.W., W.K., T.T., and M.H. are members of the DFG Cluster of Excellence ImmunoSensation (EXC 1023).

Received: September 26, 2016
Revised: July 5, 2017
Accepted: September 20, 2017
Published: October 17, 2017

REFERENCES

Baek, J.-H., Birchmeier, C., Zenke, M., and Hieronymus, T. (2012). The HGF receptor/Met tyrosine kinase is a key regulator of dendritic cell migration in skin immunity. J. Immunol. *189*, 1699–1707.

Bald, T., Quast, T., Landsberg, J., Rogava, M., Glodde, N., Lopez-Ramos, D., Kohlmeyer, J., Riesenberg, S., van den Boorn-Konijnenberg, D., Hömig-Hölzel, C., et al. (2014a). Ultraviolet-radiation-induced inflammation promotes angiotropism and metastasis in melanoma. Nature *507*, 109–113.

Bald, T., Landsberg, J., Lopez-Ramos, D., Renn, M., Glodde, N., Jansen, P., Gaffal, E., Steitz, J., Tolba, R., Kalinke, U., et al. (2014b). Immune cell-poor melanomas benefit from PD-1 blockade after targeted type I IFN activation. Cancer Discov. *4*, 674–687.

Benci, J.L., Xu, B., Qiu, Y., Wu, T.J., Dada, H., Twyman-Saint Victor, C., Cucolo, L., Lee, D.S.M., Pauken, K.E., Huang, A.C., et al. (2016). Tumor interferon signaling regulates a multigenic resistance program to immune checkpoint blockade. Cell *167*, 1540–1554.

Benkhoucha, M., Santiago-Raber, M.-L., Schneiter, G., Chofflon, M., Funakoshi, H., Nakamura, T., and Lalive, P.H. (2010). Hepatocyte growth factor inhibits CNS autoimmunity by inducing tolerogenic dendritic cells and CD25+Foxp3+ regulatory T cells. Proc. Natl. Acad. Sci. USA *107*, 6424–6429.

Blaisdell, A., Crequer, A., Columbus, D., Daikoku, T., Mittal, K., Dey, S.K., and Erlebacher, A. (2015). Neutrophils oppose uterine epithelial carcinogenesis via debridement of hypoxic tumor cells. Cancer Cell *28*, 785–799.

Bowers, N.L., Helton, E.S., Huijbregts, R.P.H., Goepfert, P.A., Heath, S.L., and Hel, Z. (2014). Immune suppression by neutrophils in HIV-1 infection: role of PD-L1/PD-1 pathway. PLoS Pathog. *10*, e1003993.

Campbell, E.L., Bruyninckx, W.J., Kelly, C.J., Glover, L.E., McNamee, E.N., Bowers, B.E., Bayless, A.J., Scully, M., Saeedi, B.J., Golden-Mason, L., et al. (2014). Transmigrating neutrophils shape the mucosal microenvironment through localized oxygen depletion to influence resolution of inflammation. Immunity *40*, 66–77.

Chtanova, T., Schaeffer, M., Han, S.-J., van Dooren, G.G., Nollmann, M., Herzmark, P., Chan, S.W., Satija, H., Camfield, K., Aaron, H., et al. (2008). Dynamics of neutrophil migration in lymph nodes during infection. Immunity *29*, 487–496.

Coffelt, S.B., Kersten, K., Doornebal, C.W., Weiden, J., Vrijland, K., Hau, C.-S., Verstegen, N.J.M., Ciampricotti, M., Hawinkels, L.J.A.C., Jonkers, J., and de Visser, K.E. (2015). IL-17-producing γδ T cells and neutrophils conspire to promote breast cancer metastasis. Nature *522*, 345–348.

Crompton, J.G., Sukumar, M., Roychoudhuri, R., Clever, D., Gros, A., Eil, R.L., Tran, E., Hanada, K., Yu, Z., Palmer, D.C., et al. (2015). Akt inhibition enhances expansion of potent tumor-specific lymphocytes with memory cell characteristics. Cancer Res. *75*, 296–305.

Ebert, P.J.R., Cheung, J., Yang, Y., McNamara, E., Hong, R., Moskalenko, M., Gould, S.E., Maecker, H., Irving, B.A., Kim, J.M., et al. (2016). MAP kinase inhibition promotes T cell and anti-tumor activity in combination with PD-L1 checkpoint blockade. Immunity *44*, 609–621.

Eickhoff, S., Brewitz, A., Gerner, M.Y., Klauschen, F., Komander, K., Hemmi, H., Garbi, N., Kaisho, T., Germain, R.N., and Kastenmüller, W. (2015). Robust anti-viral immunity requires multiple distinct T cell-dendritic cell interactions. Cell *162*, 1322–1337.

Eruslanov, E.B., Bhojnagarwala, P.S., Quatromoni, J.G., Stephen, T.L., Ranganathan, A., Deshpande, C., Akimova, T., Vachani, A., Litzky, L., Hancock, W.W., et al. (2014). Tumor-associated neutrophils stimulate T cell responses in early-stage human lung cancer. J. Clin. Invest. *124*, 5466–5480.

Ferrucci, P.F., Gandini, S., Battaglia, A., Alfieri, S., Di Giacomo, A.M., Giannarelli, D., Cappellini, G.C.A., De Galitiis, F., Marchetti, P., Amato, G., et al. (2015). Baseline neutrophil-to-lymphocyte ratio is associated with outcome of ipilimumab-treated metastatic melanoma patients. Br. J. Cancer *112*, 1904–1910.

Finisguerra, V., Di Conza, G., Di Matteo, M., Serneels, J., Costa, S., Thompson, A.A.R., Wauters, E., Walmsley, S., Prenen, H., Granot, Z., et al. (2015). MET is required for the recruitment of anti-tumoural neutrophils. Nature *522*, 349–353.

Finisguerra, V., Prenen, H., and Mazzone, M. (2016). Preclinical and clinical evaluation of MET functions in cancer cells and in the tumor stroma. Oncogene *35*, 5457–5467.

Fridlender, Z.G., Sun, J., Kim, S., Kapoor, V., Cheng, G., Ling, L., Worthen, G.S., and Albelda, S.M. (2009). Polarization of tumor-associated neutrophil phenotype by TGF-beta: "N1" versus "N2" TAN. Cancer Cell *16*, 183–194.

Gabrilovich, D.I., Ostrand-Rosenberg, S., and Bronte, V. (2012). Coordinated regulation of myeloid cells by tumours. Nat. Rev. Immunol. *12*, 253–268.

Gebhardt, C., Sevko, A., Jiang, H., Lichtenberger, R., Reith, M., Tarnanidis, K., Holland-Letz, T., Umansky, L., Beckhove, P., Sucker, A., et al. (2015). Myeloid cells and related chronic inflammatory factors as novel predictive markers in melanoma treatment with ipilimumab. Clin. Cancer Res. *21*, 5453–5459.

Gerrard, T.L., Cohen, D.J., and Kaplan, A.M. (1981). Human neutrophil-mediated cytotoxicity to tumor cells. J. Natl. Cancer Inst. *66*, 483–488.

Granot, Z., Henke, E., Comen, E.A., King, T.A., Norton, L., and Benezra, R. (2011). Tumor entrained neutrophils inhibit seeding in the premetastatic lung. Cancer Cell *20*, 300–314.

Graveel, C.R., Tolbert, D., and Vande Woude, G.F. (2013). MET: a critical player in tumorigenesis and therapeutic target. Cold Spring Harb. Perspect. Biol. *5*, a009209.

Grenier, A., Chollet-Martin, S., Crestani, B., Delarche, C., El Benna, J., Boutten, A., Andrieu, V., Durand, G., Gougerot-Pocidalo, M.-A., Aubier, M., and Dehoux, M. (2002). Presence of a mobilizable intracellular pool of

hepatocyte growth factor in human polymorphonuclear neutrophils. Blood *99*, 2997–3004.

Hampton, H.R., Bailey, J., Tomura, M., Brink, R., and Chtanova, T. (2015). Microbe-dependent lymphatic migration of neutrophils modulates lymphocyte proliferation in lymph nodes. Nat. Commun. *6*, 7139.

Hasenberg, A., Hasenberg, M., Männ, L., Neumann, F., Borkenstein, L., Stecher, M., Kraus, A., Engel, D.R., Klingberg, A., Seddigh, P., et al. (2015). Catchup: a mouse model for imaging-based tracking and modulation of neutrophil granulocytes. Nat. Methods *12*, 445–452.

Hattori, N., Mizuno, S., Yoshida, Y., Chin, K., Mishima, M., Sisson, T.H., Simon, R.H., Nakamura, T., and Miyake, M. (2004). The plasminogen activation system reduces fibrosis in the lung by a hepatocyte growth factor-dependent mechanism. Am. J. Pathol. *164*, 1091–1098.

Henry, C.M., Sullivan, G.P., Clancy, D.M., Afonina, I.S., Kulms, D., and Martin, S.J. (2016). Neutrophil-derived proteases escalate inflammation through activation of IL-36 family cytokines. Cell Rep. *14*, 708–722.

Hikono, H., Kohlmeier, J.E., Takamura, S., Wittmer, S.T., Roberts, A.D., and Woodland, D.L. (2007). Activation phenotype, rather than central- or effector-memory phenotype, predicts the recall efficacy of memory CD8+ T cells. J. Exp. Med. *204*, 1625–1636.

Hölzel, M., Bovier, A., and Tüting, T. (2013). Plasticity of tumour and immune cells: a source of heterogeneity and a cause for therapy resistance? Nat. Rev. Cancer *13*, 365–376.

Huh, C.-G., Factor, V.M., Sánchez, A., Uchida, K., Conner, E.A., and Thorgeirsson, S.S. (2004). Hepatocyte growth factor/c-met signaling pathway is required for efficient liver regeneration and repair. Proc. Natl. Acad. Sci. USA *101*, 4477–4482.

Jalili, A., Shirvaikar, N., Marquez-Curtis, L.A., Turner, A.R., and Janowska-Wieczorek, A. (2010). The HGF/c-Met axis synergizes with G-CSF in the mobilization of hematopoietic stem/progenitor cells. Stem Cells Dev. *19*, 1143–1151.

Kamenyeva, O., Boularan, C., Kabat, J., Cheung, G.Y.C., Cicala, C., Yeh, A.J., Chan, J.L., Periasamy, S., Otto, M., and Kehrl, J.H. (2015). Neutrophil recruitment to lymph nodes limits local humoral response to *Staphylococcus aureus*. PLoS Pathog. *11*, e1004827.

Kastenmüller, W., Torabi-Parizi, P., Subramanian, N., Lämmermann, T., and Germain, R.N. (2012). A spatially-organized multicellular innate immune response in lymph nodes limits systemic pathogen spread. Cell *150*, 1235–1248.

Kohlmeyer, J., Cron, M., Landsberg, J., Bald, T., Renn, M., Mikus, S., Bondong, S., Wikasari, D., Gaffal, E., Hartmann, G., and Tüting, T. (2009). Complete regression of advanced primary and metastatic mouse melanomas following combination chemoimmunotherapy. Cancer Res. *69*, 6265–6274.

Landsberg, J., Kohlmeyer, J., Renn, M., Bald, T., Rogava, M., Cron, M., Fatho, M., Lennerz, V., Wölfel, T., Hölzel, M., and Tüting, T. (2012). Melanomas resist T-cell therapy through inflammation-induced reversible dedifferentiation. Nature *490*, 412–416.

Laubach, V.E., Shesely, E.G., Smithies, O., and Sherman, P.A. (1995). Mice lacking inducible nitric oxide synthase are not resistant to lipopolysaccharide-induced death. Proc. Natl. Acad. Sci. USA *92*, 10688–10692.

Law, C.W., Chen, Y., Shi, W., and Smyth, G.K. (2014). voom: Precision weights unlock linear model analysis tools for RNA-seq read counts. Genome Biol. *15*, R29.

Liao, Y., Smyth, G.K., and Shi, W. (2013). The Subread aligner: fast, accurate and scalable read mapping by seed-and-vote. Nucleic Acids Res. *41*, e108.

Liu, X., Wang, Q., Yang, G., Marando, C., Koblish, H.K., Hall, L.M., Fridman, J.S., Behshad, E., Wynn, R., Li, Y., et al. (2011). A novel kinase inhibitor, INCB28060, blocks c-MET-dependent signaling, neoplastic activities, and cross-talk with EGFR and HER-3. Clin. Cancer Res. *17*, 7127–7138.

Liu, J., Blake, S.J., Yong, M.C.R., Harjunpää, H., Ngiow, S.F., Takeda, K., Young, A., O'Donnell, J.S., Allen, S., Smyth, M.J., and Teng, M.W. (2016). Improved efficacy of neoadjuvant compared to adjuvant immunotherapy to eradicate metastatic disease. Cancer Discov. *6*, 1382–1399.

Manz, M.G., and Boettcher, S. (2014). Emergency granulopoiesis. Nat. Rev. Immunol. *14*, 302–314.

Mishalian, I., Bayuh, R., Levy, L., Zolotarov, L., Michaeli, J., and Fridlender, Z.G. (2013). Tumor-associated neutrophils (TAN) develop pro-tumorigenic properties during tumor progression. Cancer Immunol. Immunother. *62*, 1745–1756.

Nagato, T., Lee, Y.-R., Harabuchi, Y., and Celis, E. (2014). Combinatorial immunotherapy of polyinosinic-polycytidylic acid and blockade of programmed death-ligand 1 induce effective CD8 T-cell responses against established tumors. Clin. Cancer Res. *20*, 1223–1234.

Ngiow, S.F., Young, A., Jacquelot, N., Yamazaki, T., Enot, D., Zitvogel, L., and Smyth, M.J. (2015). A threshold level of intratumor CD8+ T-cell PD1 expression dictates therapeutic response to anti-PD1. Cancer Res. *75*, 3800–3811.

Nicolás-Ávila, J.Á., Adrover, J.M., and Hidalgo, A. (2017). Neutrophils in homeostasis, immunity, and cancer. Immunity *46*, 15–28.

Okunishi, K., Dohi, M., Nakagome, K., Tanaka, R., Mizuno, S., Matsumoto, K., Miyazaki, J., Nakamura, T., and Yamamoto, K. (2005). A novel role of hepatocyte growth factor as an immune regulator through suppressing dendritic cell function. J. Immunol. *175*, 4745–4753.

Pekarek, L.A., Starr, B.A., Toledano, A.Y., and Schreiber, H. (1995). Inhibition of tumor growth by elimination of granulocytes. J. Exp. Med. *181*, 435–440.

Pennacchietti, S., Michieli, P., Galluzzo, M., Mazzone, M., Giordano, S., and Comoglio, P.M. (2003). Hypoxia promotes invasive growth by transcriptional activation of the met protooncogene. Cancer Cell *3*, 347–361.

Riesenberg, S., Groetchen, A., Siddaway, R., Bald, T., Reinhardt, J., Smorra, D., Kohlmeyer, J., Renn, M., Phung, B., Aymans, P., et al. (2015). MITF and c-Jun antagonism interconnects melanoma dedifferentiation with pro-inflammatory cytokine responsiveness and myeloid cell recruitment. Nat. Commun. *6*, 8755.

Robinson, M.D., McCarthy, D.J., and Smyth, G.K. (2010). edgeR: a Bioconductor package for differential expression analysis of digital gene expression data. Bioinformatics *26*, 139–140.

Sagiv, J.Y., Michaeli, J., Assi, S., Mishalian, I., Kisos, H., Levy, L., Damti, P., Lumbroso, D., Polyansky, L., Sionov, R.V., et al. (2015). Phenotypic diversity and plasticity in circulating neutrophil subpopulations in cancer. Cell Rep. *10*, 562–573.

Sarkar, S., Kalia, V., Haining, W.N., Konieczny, B.T., Subramaniam, S., and Ahmed, R. (2008). Functional and genomic profiling of effector CD8 T cell subsets with distinct memory fates. J. Exp. Med. *205*, 625–640.

Shen, M., Hu, P., Donskov, F., Wang, G., Liu, Q., and Du, J. (2014). Tumor-associated neutrophils as a new prognostic factor in cancer: a systematic review and meta-analysis. PLoS ONE *9*, e98259.

Shojaei, F., Lee, J.H., Simmons, B.H., Wong, A., Esparza, C.O., Plumlee, P.A., Feng, J., Stewart, A.E., Hu-Lowe, D.D., and Christensen, J.G. (2010). HGF/c-Met acts as an alternative angiogenic pathway in sunitinib-resistant tumors. Cancer Res. *70*, 10090–10100.

Singhal, S., Bhojnagarwala, P.S., O'Brien, S., Moon, E.K., Garfall, A.L., Rao, A.S., Quatromoni, J.G., Stephen, T.L., Litzky, L., Deshpande, C., et al. (2016). Origin and role of a subset of tumor-associated neutrophils with antigen-presenting cell features in early-stage human lung cancer. Cancer Cell *30*, 120–135.

Spitzer, M.H., Carmi, Y., Reticker-Flynn, N.E., Kwek, S.S., Madhireddy, D., Martins, M.M., Gherardini, P.F., Prestwood, T.R., Chabon, J., Bendall, S.C., et al. (2017). Systemic immunity is required for effective cancer immunotherapy. Cell *168*, 487–502.

Templeton, A.J., McNamara, M.G., Šeruga, B., Vera-Badillo, F.E., Aneja, P., Ocaña, A., Leibowitz-Amit, R., Sonpavde, G., Knox, J.J., Tran, B., et al. (2014). Prognostic role of neutrophil-to-lymphocyte ratio in solid tumors: a systematic review and meta-analysis. J. Natl. Cancer Inst. *106*, dju124.

Tesio, M., Golan, K., Corso, S., Giordano, S., Schajnovitz, A., Vagima, Y., Shivtiel, S., Kalinkovich, A., Caione, L., Gammaitoni, L., et al. (2011).

Enhanced c-Met activity promotes G-CSF-induced mobilization of hematopoietic progenitor cells via ROS signaling. Blood *117*, 419–428.

Trusolino, L., Bertotti, A., and Comoglio, P.M. (2010). MET signalling: principles and functions in development, organ regeneration and cancer. Nat. Rev. Mol. Cell Biol. *11*, 834–848.

Voehringer, D., Koschella, M., and Pircher, H. (2002). Lack of proliferative capacity of human effector and memory T cells expressing killer cell lectinlike receptor G1 (KLRG1). Blood *100*, 3698–3702.

Wculek, S.K., and Malanchi, I. (2015). Neutrophils support lung colonization of metastasis-initiating breast cancer cells. Nature *528*, 413–417.

Yang, C.-W., and Unanue, E.R. (2013). Neutrophils control the magnitude and spread of the immune response in a thromboxane A2-mediated process. J. Exp. Med. *210*, 375–387.

Yang, C.-W., Strong, B.S.I., Miller, M.J., and Unanue, E.R. (2010). Neutrophils influence the level of antigen presentation during the immune response to protein antigens in adjuvants. J. Immunol. *185*, 2927–2934.

STAR★METHODS

KEY RESOURCES TABLE

REAGENT or RESOURCE	SOURCE	IDENTIFIER
Antibodies		
Rabbit monoclonal p44/42 MAPK (Erk1/2)	Cell Signaling	Cat#9102; RRID: AB_330744
Mouse monoclonal phospho-ERK (Clone E-4)	Santa Cruz	Cat#sc-7383; RRID: AB_627545
Rabbit monoclonal phospho-p44/42 MAPK (Erk1/2) (Thr202/Tyr204; Clone D13.14.4E)	Cell Signaling	Cat#4370; RRID: AB_2315112
Mouse monoclonal Akt (pan) (Clone 40D4)	Cell Signaling	Cat#2920; RRID: AB_1147620
Rabbit monoclonal Akt (pan) (Clone C67E7)	Cell Signaling	Cat#4691; RRID: AB_915783
Rabbit monoclonal phospho-Akt (Ser473; Clone D9E)	Cell Signaling	Cat#4060; RRID: AB_2315049
Mouse monoclonal β-Actin (Clone C4)	Santa Cruz	Cat#sc-47778; RRID: AB_626632
Mouse monoclonal c-MET (Clone B-2)	Santa Cruz	Cat#sc-8057; RRID: AB_673755
Rabbit monoclonal phospho-MET (Tyr1234/1235; Clone D26)	Cell Signaling	Cat#3077S; RRID: AB_2143884
Goat polyclonal gp100	Novus Biologicals	Cat#NB100-41098 RRID: AB_2254576
IRDye 680RD Donkey anti-Mouse IgG (H+L)	LI-COR Biosciences	Cat#926-68072; RRID: AB_10953628
IRDye 800CW Donkey anti-Mouse IgG (H+L)	LI-COR Biosciences	Cat#926-32212; RRID: AB_621847
IRDye 800CW Donkey anti-Rabbit IgG (H+L)	LI-COR Biosciences	Cat#926-32213; RRID: AB_621848
IRDye 800CW Donkey anti-Goat IgG (H+L)	LI-COR Biosciences	Cat#926-32214; RRID: AB_621846
IRDye 680LT Donkey (polyclonal) anti-Rabbit IgG (H+L)	LI-COR Biosciences	Cat#926-68023; RRID: AB_10706167
Anti-Mouse CD16/CD32 (Clone 93)	Biolegend	Cat#101302; RRID: AB_312801
Anti-Mouse CD45 PerCp (Clone 30-F11)	BD Bioscience	Cat#557235; RRID: AB_396609
Anti-Mouse CD45.2 APC/Cy7 (Clone 104)	Biolegend	Cat#109824; RRID: AB_830789
Anti-Mouse CD45 Brilliant Violet 421 (Clone 30-F11)	Biolegend	Cat#103133: RRID: AB_10899570
Anti-Mouse CD8 PE (Clone 53-6.7)	BD PharMingen	Cat#553033; RRID: AB_394571
Anti-Rat CD90.1 Alexa Flour 647 (Clone OX-7)	Biolegend	Cat#202508; RRID: AB_492884
Anti-Rat CD90.1 PerCP (Clone OX-7)	BD Bioscience	Cat#557266; RRID: AB_396611
Anti-Mouse/Human CD11b FITC (Clone M1/70)	Biolegend	Cat#101206; RRID: AB_312789
Anti-Mouse Ly6G PE (Clone 1A8)	BD Bioscience	Cat#551461; RRID: AB_394208
Anti-Mouse Ly6C APC (Clone AL-21)	BD Bioscience	Cat#560595; RRID: AB_1727554
Anti-Mouse/Human Klrg1 PerCP/Cy5.5 (Clone 2F1)	Biolegend	Cat#138418; RRID: AB_2563015
Anti-Mouse CD279 (PD-1) FITC (Clone J43)	Thermo Fisher Scientific	Cat#11-9985-82; RRID: AB_465472
Anti-mouse monoclonal CD223 (LAG-3) eFluor450 (Clone eBioC9B7W)	ThermoFisher Scientific	Cat#48-2231-82; RRID: AB_11149866
Anti-Mouse CD8a BV711 (Clone 53-6.7)	Biolegend	Cat#100748; RRID: AB_2562100
Anti-Mouse TCRb PerCP/Cy5.5 (Clone H57-597)	Biolegend	Cat#109228; RRID: AB_1575173
Anti-Mouse Klrg1 PECy7 (Clone 2F1)	eBioscience	Cat#25-5893-82; RRID: AB_1518768
Anti-Mouse CD274 (PD-L1) BV711 (Clone B7-H1))	Biolegend	Cat#124319; RRID: AB_2563619
Anti-Mouse/Human Ki67 Alexa Fluor 647 (Clone B56)	BD Bioscience	Cat#561126
Anti-Mouse/Human GranzymeB Pacific Blue (Clone GB11)	Biolegend	Cat#515408; RRID: AB_2562196

(*Continued on next page*)

Continued

REAGENT or RESOURCE	SOURCE	IDENTIFIER
H-2Ld tetramer to peptide SPSYVYHQF APC	National Institutes of Health (NIH Tetramer Core Facility)	MuLV env gp70 423-431
Anti-Mouse c-MET (HGFr)	RnD	Cat#AF527; RRID: AB_355414
Polyclonal rabbit anti-goat IgG/biotinylated	Agilent (DAKO)	Cat#E046601-2
Streptavidin-APC	BD Bioscience	Cat#554067; RRID: AB_10050396
Streptavidin-APC-eFlour 780	Thermo Fisher Scientific	Cat# 47-4317-82; RRID: AB_10366688
Anti-Mouse PD-L1 PE (Clone MIH5)	BD Bioscience	Cat#558091; RRID: AB_397018
Mouse Hematopoietic Lineage Biotin Panel	Thermo Fisher Scientific	Cat# 88-7774-75; RRID: AB_476399
Anti-Mouse monoclonal Granzyme B FITC (Clone NGZB)	Thermo Fisher Scientific	Cat#11-8898-82; RRID: AB_10733414
Monoclonal anti- Ki67 FITC (Clone SolA15)	Thermo Fisher Scientific	Cat#11-5698-82; RRID: AB_11151330
Anti-Mouse IFNy APC (Clone XMG1.2)	Thermo Fisher Scientific	Cat#17-7311-82; RRID: AB_469504
Anti-Mouse CD34-FITC (Clone RAM34)	Thermo Fisher Scientific	Cat#11-0341-82; RRID: AB_465021
Anti-Mouse Sca-1 PE-Cy7 (Clone D7)	Thermo Fisher Scientific	Cat#25-5981-82; RRID: AB_469669
Anti-Mouse CD117 (c-Kit) APC (Clone 2B8)	Thermo Fisher Scientific	Cat#17-1171-82; RRID: AB_469430
Anti-Human/Mouse CD45R PerCP-Cy5.5	Thermo Fisher Scientific	Cat#45-0452-82; RRID: AB_1107006
B220 PerCP/Cy5.5 (Clone R43-6B2)	Thermo Fisher Scientific	Cat# 45-0452-82; RRID: AB_1107006
Anti-CD16/32-eF450 (Clone 93)	Thermo Fisher Scientific	Cat#48-0161-82; RRID: AB_1272191
Anti-Mouse CD3e PE-Cy7 (Clone 145-2C11)	Thermo Fisher Scientific	Cat#25-0031-82; RRID: AB_469572
Anti-Mouse CD11b eFlour450 (M1/70)	eBioscience	Cat#48-0112-82; RRID: AB_1582236
Anti-Mouse Ly-6A/E PE-Cy7 (Sca-1; Clone D7),	eBioscience	Cat#25-5981-82; RRID: AB_469669
anti-mouse-PD-L1 (Clone 10F.9G2)	Bioxcell	Cat#BE0101 RRID:AB_10949073
anti-GFP polyclonal Alexa Fluor 488	Thermo Fisher Scientific	Cat#A-21311; RRID: AB_221477
Cell Proliferation Dye eFluor 670	Thermo Fisher Scientific	Cat#65-0840-85
In vivo Mab anti-mouse PD-1 (Clone RMP1-14)	BioXcell	Cat#BE0146; RRID: AB_10949053
Zombie Yellow Fixable Viability Kit	Biolegend	Cat#423103
Zombie Aqua Fixable Viability Kit	Biolegend	Cat#423101
In vivo Mab rat IgG2a Isotype control (Clone 2A3)	BioXcell	Cat#BE0089; RRID: AB_1107769
In vivo Mab anti-mouse CD137 (4-1bb)	Bioxcell	Cat#BE0239; RRID: AB_2687721
Bacterial and Virus Strains		
Recombinant adenoviral vector Ad-gp100	Kohlmeyer et al., 2009	N/A
Biological Samples		
Human blood and serum samples	Skin Cancer Centre, University Medical Center Mannheim, Germany (Biobank core facility)	N/A
Human blood and serum samples	Skin Cancer Centre, University Hospital Bonn, Germany (Biobank core facility)	N/A
Human blood and serum samples	Melanoma Institute Australia, Sydney, Australia	N/A
Chemicals, Peptides, and Recombinant Proteins		
c-MET inhibitor capmatinib (INC280)	Selleck Chemicals	Cat#S2788
c-MET inhibitor capmatinib	provided by Novartis	N/A
c-MET inhibitor PF-04217903	Selleck Chemicals	Cat#S1094
Cyclophosphamide	Endoxan, Baxter	Cat#01469644
PolyI:C (HMW)	Invivogen	Cat#tlrl-pic
H2-D^b binding peptide KVPRNQDWL ($gp100_{aa25–33}$)	JPT	N/A
Recombinant human IL-2 (Aldesleukin)	Novartis Pharma	PZN:02238131

(*Continued on next page*)

Continued

REAGENT or RESOURCE	SOURCE	IDENTIFIER
Recombinant murine IFNy	Peprotech	Cat#315-05
Recombinant murine TNFα	Peprotech	Cat#315-01A
Critical Commercial Assays		
M-PER mammalian protein reagent	Fermentas	Cat#78501
Protease inhibitor cocktail	Thermo Fisher Scientific	Cat#78430
Pierce BCA protein assay	Thermo Fisher Scientific	Cat#23225
Mouse/rat HGF Quantikine ELISA kit	RnD	Cat#MHG00
Human HGF Quantikine ELISA kit	RnD	Cat#DHG00
Fixation/Permeabilization Solution Kit	BD	Cat#554714
Foxp3 / Transcription Factor Staining Buffer Set	eBioscience	Cat#00-5523-00
Deposited Data		
Raw 3′mRNA-Seq data	EBI ENA: ERP023772/ PRJEB21513	http://www.ebi.ac.uk/ena/data/view/ERP023772 or http://www.ebi.ac.uk/ena/data/view/PRJEB21513
Experimental Models: Cell Lines		
Mouse: HCmel12 melanoma	Established in the laboratory of T.T. (Bald et al., 2014a)	N/A
Mouse: B16F1 melanoma	Obtained by T.T. from ATCC	ATCC CRL-6323
Mouse: LLC lung cancer	University of Bonn, Germany; provided by J. vd. Boorn, Inst. f. Clinical Chemistry and Clinical Pharmacology	N/A
Mouse: MC38 colon	QIMR Berghofer, Brisbane, Australia; M.J.S. laboratory	N/A
Mouse: 4T1.2 breast cancer	QIMR Berghofer, Brisbane, Australia; M.J.S. laboratory	N/A
Experimental Models: Organisms/Strains		
Mouse: C57BL/6J (H-2D^{b})	Janvier LABS	sc-C57J
Mouse: C57BL/6J (H-2D^{b})	Charles River	JAX 000664
Mouse: C57BL/6J (H-2D^{b})	Walter and Eliza Hall Institute for Medical Research	N/A
Mouse: BALB/c	Walter and Eliza Hall Institute	N/A
Mouse: *Hgf-Cdk4*$^{(R24C)}$	Kohlmeyer et al., 2009; laboratory of T.T.	N/A
Mouse: TCR tg Pmel-1	Jackson Laboratory	Cat# 005023
Mouse: GFP-TCRtg Pmel-1	This paper	N/A
Mouse: *Met*$^{exon16fl/fl}$	Laboratory of M.M.	N/A
Mouse: hMRP8-*Cre*-ires/*GFP*x*Met*$^{exon16fl/fl}$ (*Met*$^{exon16\Delta NEU}$)	Finisguerra et al., 2015; Huh et al., 2004	N/A
Mouse: Ly6G^{Cre}ROSA26$^{LSL\text{-}tdTomato}$	Hasenberg et al., 2015	N/A
Mouse: Nos2-deficient	Laubach et al., 1995	N/A
Oligonucleotides		
CPG Oligo 1826; 5′-T*C*C*A*T*G*A*C*G*T* T*C*C*T*G*A*C*G*T*T-3′	Biomers	N/A
Software and Algorithms		
FlowJo v10	Tree Star, Inc.	https://www.flowjo.com/
Imaris	Bitplane	http://www.bitplane.com/
GraphPad Prism v7	GraphPad	https://www.graphpad.com/scientific-software/prism/
R	R developer team	https://cran.r-project.org/
Rstudio	Rstudio	https://www.rstudio.com/
Bioconductor - R-based computing platform	Bioconductor developer team	https://bioconductor.org/

(*Continued on next page*)

Continued

REAGENT or RESOURCE	SOURCE	IDENTIFIER
Rsubread - Bioconductor package	Liao et al., 2013	https://bioconductor.org/packages/release/bioc/html/Rsubread.html
edgeR - Bioconductor package	Robinson et al., 2010	https://bioconductor.org/packages/release/bioc/html/edgeR.html
org.Mm.eg.db - Bioconductor package, Genome wide annotation for Mouse. R package version 3.4.1.	Package author: Carlson, M.	http://bioconductor.org/packages/release/data/annotation/html/org.Mm.eg.db.html
heatmap.3 - An Improved Heatmap Package. R package.	Package authors: Zhao, S., Guo, Y., Sheng, Q., Shyr, Y.	https://CRAN.R-project.org/packages/heatmap3/index.html
coin - Conditional Inference Procedures in a Permutation Test Framework. R package	Package authors: Hothorn, T., Hornik, K., van de Wiel, M.A., Winell, H., Zeileis, A.	https://CRAN.R-project.org/packages/coin/index.html
cgdsr - R-Based API for Accessing the MSKCC Cancer Genomics Data Server	Package author: Jacobsen, A.	https://CRAN.R-project.org/packages/cgdsr/index.html
Voom - algorithm (implemented in limma)	Law et al., 2014	https://doi.org/10.1186/gb-2014-15-2-r29 https://bioconductor.org/packages/release/bioc/html/limma.html
RNA-seq algorithm	As described by Shi et al., Bioinformatics Division, WEHI, Melbourne, Australia	http://bioinf.wehi.edu.au/RNAseqCaseStudy/
Moving Average plots	Riesenberg et al., 2015	https://images.nature.com/original/nature-assets/ncomms/2015/151104/ncomms9755/extref/ncomms9755-s9.txt

CONTACT FOR REAGENT AND RESOURCE SHARING

Further information and requests for reagents may be directed to, and will be fulfilled by the Lead Contact Michael Hölzel (michael.hoelzel@ukbonn.de).

EXPERIMENTAL MODEL AND SUBJECT DETAILS

Mice

C57BL/6J mice (*H-2D*^{b}) were purchased from Charles River, Janvier or Walter and Eliza Hall Institute for Medical Research. BALB/c mice were purchased from the Walter and Eliza Hall Institute for Medical Research. Melanoma prone *Hgf-Cdk4*$^{(R24C)}$ mice were bred as described previously (Kohlmeyer et al., 2009; Landsberg et al., 2012). TCR-transgenic Pmel-1 mice expressing an $\alpha\beta$ TCR specific for amino acids 25–33 of human and mouse gp100 presented by H2-D^{b} were bred as described previously (Landsberg et al., 2012). GFP expressing Pmel-1 mice were generated by crossing Pmel-1 mice with Ubc-GFP transgenic mice. *Met*$^{exon16fl/fl}$ and hMRP8-*Cre*-ires/*GFP*x*Met*$^{exon16fl/fl}$ (*Met*$^{exon16\Delta NEU}$) mice were described previously (Finisguerra et al., 2015; Huh et al., 2004). Ly6G^{Cre}ROSA26$^{LSL\text{-}tdTomato}$ (Catchup$^{IVM\text{-}red}$) and *Nos2*-deficient mice were bred as described previously (Hasenberg et al., 2015; Laubach et al., 1995). All animals were maintained under specific pathogen-free conditions in individually ventilated cages and experiments were performed with 6-8 week old mice. Age and sex matched cohorts of mice bearing successfully transplanted tumors were randomly allocated to the different experimental groups at the start of each experiment. All animal experiments were approved by the responsible authorities (Landesverwaltungsamt, SA, and LANUV, NRW, Germany; QIMR Berghofer AEC, Queensland, Australia and Animal Care and Research Advisory Committee KU Leuven, Leuven, Belgium) and were performed according to the institutional and national guidelines for the care and use of laboratory animals.

Cell lines

The melanoma cell line HCmel12 was established from a primary melanoma in the *Hgf-Cdk4*^{R24C} mouse model by serial transplantation in our laboratory as described previously (Bald et al., 2014a). B16F1 was originally obtained from ATCC and this model was previously used for immunotherapeutic studies by our group (Kohlmeyer et al., 2009). Syngeneic MC38 mouse colon adenocarcinoma cells were used as described previously (Ngiow et al., 2015). LLC mouse lung cancer cells were provided by J.v.d. Boorn (Institute for Clinical Chemistry and Clinical Pharmacology, Bonn). BALB/c-derived 4T1.2 mammary carcinoma cells were used as described previously (Liu et al., 2016). All cell lines were routinely cultured in "complete RPMI medium," i.e., RPMI 1640 medium (Life Technologies) supplemented with 10% FCS (Biochrome), 2 mM L-glutamine, 10 mM non-essential amino acids, 1 mM HEPES

(all from Life Technologies), 20 μM 2-mercaptoethanol (Sigma), 100 IU/ml penicillin and 100 μg/ml streptomycin (Invitrogen) in a humidified incubator with 5% CO_2. All cell lines used in this study were routinely tested for mycoplasma contamination by PCR on a monthly basis.

Primary cell cultures

For *in vitro* studies single cell suspensions of bone marrow neutrophils and Pmel-1 T cells isolated from spleens of Pmel-1 TCRtg mice were cultured in "complete RPMI medium," i.e., RPMI 1640 medium (Thermo Fisher Scientific) supplemented with 10% FCS (Biochrome), 2 mM L-glutamine, 10 mM non-essential amino acids, 1 mM HEPES (all from Life Technologies), 20 μM 2-mercaptoethanol (Sigma), 100 IU/ml penicillin and 100 μg/ml streptomycin (Invitrogen) in a humidified incubator with 5% CO_2. Pmel-1 T cell culture medium was additionally supplemented with 30cU/ml recombinant human IL-2 (Aldesleukin) and 1 μg/ml of the H2-D^b binding peptide KVPRNQDWL ($gp100_{aa25–33}$).

Human blood and serum samples

Patient samples (blood and serum) and clinical data were obtained with the approval of institutional Ethics Committee boards and patients' consents at the Skin Cancer Centre, University Medical Center Mannheim, Germany, at the Skin Cancer Centre of the University Hospital Bonn, Germany and at the Melanoma Institute Australia, Sydney, Australia. At the clinical centers serum samples were collected on a routinely basis for institutional biobanking programs and were made available for our explorative retrospective analyses. Serum aliquots were stored at −80°C until analysis in freezers with temperature surveillance. If applicable to our retrospective study, we followed the REMARK guidelines for tumor marker prognostic studies. All patients received either pembrolizumab or nivolumab as anti-PD1 therapy for their confirmed diagnosis of stage IV melanoma according to the 2009 AJCC melanoma staging and classification (Table S1). Patients had not any specific melanoma therapy during the previous 21 days or concomitant systemic therapy for melanoma. Treatment efficacy was assessed using contrast-enhanced CT/MRI or PET-CT at around week 12 after the first anti-PD-1 infusions. A clinical response was defined as complete response (CR), partial response (PR) and stable disease (SD) based on immune-related response criteria (irRC).

METHOD DETAILS

Cell growth assays

Tumor cells were plated at low density (5000 cells for HCmel12, MC38 and LLC and 2000 cells for B16F1 and 4T1.2) in 12-well plates and treated with capmatinib (INC280) or PF-04217903 (both from Selleck Chemicals) at indicated concentrations or vehicle control for 6 days. Dishes were stained with a standard crystal violet staining procedure. In brief, cells were washed with PBS, fixed in 4% formaldehyde solution and stained with 0.05% crystal violet in water for 30 min. Stained dishes were washed three times with water to remove background staining. Colonies were scanned and quantified using the Odyssey SA Infrared Imaging System (LICOR Biosciences).

Immunoblots

Protein lysates were prepared from cultured cells after two hours of incubation with capmatinib (INC280), PF-04217903 or vehicle control and lysed directly in Laemmli buffer (SDS loading buffer). Melanoma tissues were harvested two hours after the last administration of capmatinib. Tumor samples were lysed using the M-PER mammalian protein reagent (Fermentas) with protease inhibitors (Roche). Laemmli buffer was added to these samples after the protein concentration was spectrophotometrically measured with a Bradford-based assay using Roti-Quant (Roth) according to manufacturer's protocol. The lysates were incubated for five minutes at 95°C prior to loading. Samples were loaded and separated by SDS–PAGE gel electrophoresis and transferred to nitrocellulose membrane with 0.2 μm pore size (GE Healthcare) according to standard protocols. Blots were immunostained with p44/42 MAPK (ERK1/2) rabbit monoclonal antibody (#9102; Cell Signaling), phospho-ERK (E-4) mouse monoclonal antibody (sc-7383; Santa Cruz) for *in vitro* samples or phospho-ERK rabbit monoclonal antibody (#4370; Cell Signaling) for tumor samples, AKT (pan) (40D4) mouse monoclonal antibody (#2920; Cell Signaling) for *in vitro* samples or AKT (pan) (C67E7) rabbit monoclonal antibody (#4691; Cell Signaling) for tumor lysates; phospho-AKT (Ser473) (D9E) rabbit monoclonal antibody (#4060; Cell Signaling), β-Actin (C4) mouse monoclonal antibody (sc-47778; Santa Cruz), c-MET (B-2) mouse monoclonal antibody (sc-8057; Santa Cruz), phospho-MET (Tyr1234/1235) (D26) rabbit monoclonal antibody (#3077; Cell Signaling) and gp100 goat polyclonal antibody (#NB100-41098; Novus Biologicals). Bound antibodies were visualized with IRDye 680RD or IRDye 800CW secondary antibodies (LICOR Biosciences) for detection in the 700 nm and 800 nm channel, respectively. Blots were scanned with the Odyssey SA Infrared Imaging System (LICOR Biosciences).

Tumor transplantation experiments

Cohorts of syngeneic C57BL/6 mice were injected intracutaneously (i.c.) with either 2×10^5 HCmel12, 2×10^5 B16F1 melanoma or subcutaneously (s.c.) with either 2×10^5 LLC lung carcinoma cells or 2×10^6 MC38 colon adenocarcinoma cells in 100 μl PBS into the flanks. Cohorts of BALB/c mice were injected with 5×10^4 4T1.2 mammary carcinoma cells in 100 μl PBS into the mammary fat pad. Tumor size was measured twice weekly and recorded as mean diameter in millimeter. Tumor area was calculated in mm^2 using

the equation: A = length x width. Mice with tumors exceeding 100 mm^2 were sacrificed unless stated otherwise. Experiments were performed in groups of four or more mice and repeated at least twice.

Induction of Primary Melanomas

The development of primary melanomas on the shaved back skin of 8 weeks old *Hgf-Cdk4*^{R24C} mice was accelerated and synchronized by a single epicutaneous application of the carcinogen DMBA (100 nmol in 200 μl Aceton) as described previously (Landsberg et al., 2012). Tumor size was measured twice weekly and recorded as mean diameter in millimeter. Tumor area was calculated in mm^2 using the equation A = length x width. Mice with tumors exceeding 100 mm^2 were sacrificed unless stated otherwise. Experiments were performed in groups of five mice.

c-MET inhibition *in vivo*

For *in vivo* c-MET inhibition, tumor-bearing mice received 5 mg/kg capmatinib (INC280; purchased from Selleck Chemicals or kindly provided by Novartis), PF-04217903 (Selleck Chemicals) or vehicle intraperitoneal (i.p.) in 100 μl distilled water every 12 hours (b.i.d.) for 5 or 2 × 5 consecutive days as depicted in the manuscript.

Adoptive cell transfer (ACT) immunotherapy

ACT immunotherapy was performed as previously described (Landsberg et al., 2012). In brief, when transplanted HCmel12, B16F1 or carcinogen-induced primary melanomas reached a size of > 5 mm in diameter mice were treated with our established ACT immunotherapy and preconditioned for ACT by a single i.p. injection of 2 mg (100 mg/kg) cyclophosphamide in 100 μl PBS one day before intravenous delivery of 2 × 10^6 naive gp100-specific CD90.1$^+$CD8$^+$ Pmel-1 T cells (in 200 μl PBS) isolated from spleens of Pmel-1 TCR transgenic mice. The adoptively transferred T cells were activated *in vivo* by a single i.p. injection of 5 × 10^8 PFU of a recombinant adenoviral vector Ad-gp100 in 100 μl PBS. 50 μg of CpG 1826 (MWG Biotech) and 50 μg of polyinosinic:polycytidylic acid (poly(I:C), Invivogen) in 100 μl distilled water were injected peritumorally 3, 6, and 9 days after adoptive Pmel-1 T cell transfer. When depicted in the manuscript or figures, treatments were combined with c-MET inhibitors as described above starting with chemotherapeutic preconditioning.

Immunotherapies

When transplanted B16F1 or LLC tumors reached a size of > 5 mm in diameter, PCP immunotherapy was started. Mice received two cycles of twice weekly peritumoral injections with 50 μg poly(I:C) (Invivogen) and 50 μg CpG (MWG Biotech) in 100 μl distilled water. Therapeutic blockade of PD-1 was performed by twice weekly i.p. injections of 250 μg rat anti-mouse PD-1 IgG2a (clone RMP1-14; BioXcell) or control-rat IgG2a mAb (clone 2A3; BioXcell) in 100 μl PBS. When depicted in the manuscript treatment was combined with capmatinib (INC280) starting with the first administration of poly(I:C)/CpG. MC38-bearing mice received two treatment cycles of anti-PD1 immunotherapy (200 μg i.p. rat-anti-mouse PD-1 IgG2a; clone RMP1-14; BioXcell or control-rat IgG2a mAb; clone 2A3; BioXcell; both in 100 μl PBS) when tumors reached a size of > 5 mm in diameter as described (Ngiow et al., 2015). 4T1.2 mammary carcinoma-bearing mice received one treatment cycle of anti-PD-1 immunotherapy (200 μg i.p. rat-anti-mouse PD-1 IgG2a; clone RMP1-14; BioXcell or control-rat IgG2a mAb; clone 2A3; BioXcell; both in 100 μl PBS) in combination with anti-CD137 (100 μg i.p. rat-anti-mouse CD137; clone 3H3; BioXcell; in 100 μl PBS) when tumors reached a size of 5 mm. When depicted in the manuscript treatment was combined with capmatinib (INC280) starting with the first administration of anti-PD-1/anti-CD137 antibody. Short-term analyses were performed after the first treatment cycle.

Vitiligo scoring

The area of vitiligo-like fur depigmentation on the back of mice was scored on a scale of 0-4 as (0) 0%, (1) 1%–25%, (2) 26%–50%, (3) 51%–75% and (4) 76%–100%. Long-term surviving mice were photographed and scored by three independent investigators in a blinded fashion.

Tissue digestion

Tumor tissue, bone marrow, lymph nodes and spleens were harvested, dissociated mechanically, incubated with 1 mg/ml Collagenase D (Sigma) and 1 mg/ml DNase I (Roche) in PBS with 5% fetal bovine serum (Biochrom) at 37°C. After 30 min, tissues were passed through 70 μm cell strainers (BD Bioscience) and single suspensions were washed twice with PBS.

Flow cytometry

Immunostaining of single cell suspensions was performed according to standard protocols. Single suspensions were incubated with anti-CD16/CD32 (clone 93; Biolegend) before staining with fluorochrome-conjugated monoclonal antibodies listed in the Key Resource table. The combination of anti-CD45, anti-CD11b, anti-Ly6G, anti-c-MET (RnD), biotinylated anti-goat IgG (DAKO) and appropriate Streptavidin (BD PharMingen) was used to identify c-MET$^+$ neutrophils. Intracellular staining was carried out using the Fixation/Permeabilization Solution Kit (BD or eBioscience). Single- cell suspensions from tumors and lymph nodes were stained with antibodies against cell-surface antigens, fixed and permeabilized followed by intracellular staining. Dead cell exclusion

was performed using the Zombie Aqua™ or Zombie Yellow™ fixable viability kit (Biolegend) according to manufacturer's protocol. All data were acquired with a FACSCanto flow cytometer, LSR or LSRII flow cytometer (BD Biosciences) and analyzed using FlowJo v10 software for Windows (Tree Star, Inc.).

Analysis of absolute immune cell counts

Absolute counts of white blood cells (WBC) were obtained using the Hemavet 950 Analyzer (Drew Scientific). The relative amount of circulating immune cell subtypes (Rel_{cell}) was determined by flow cytometry. Absolute counts of $CD11b^+Ly6G^+$ neutrophils and adoptively transferred gp100 tumor antigen-specific Pmel-1 $CD90.1^+CD8^+$ T cells, gp70 tumor antigen-specific $CD8^+$ T cells or host $CD8^+$ T cells in the blood of mice were calculated using the following equation: Absolute cell counts ($10^3/\mu l$) = total WBC ($10^3/\mu l$) x Rel_{cell} (%) /100 (%). To determine neutrophil-to-Pmel-1 T cell ratio (NPR) or neutrophil-to-T cell (NTR) the absolute neutrophil counts were divided by the absolute T cell counts.

Bone marrow analysis

Bone marrow was prepared by flushing the long bones from the hind legs of sacrificed mice on day 7-10 after immunotherapy. Hematopoietic lineage discrimination of bone marrow samples was performed using B220 (Clone RA3-6B2), CD3e (Clone 145-2C11), CD11b (Clone M1/70; all from Thermo Fisher Scientific), Ly6G (Clone1A8) and Ly6C (CloneAL-21; both from BD PharMingen). The analysis of progenitor populations in bone marrow samples was performed using CD34 (Clone RAM34), Sca-1 (Clone D7), c-kit (Clone 2B8), CD16/32 (Clone 93; all from Thermo Fisher Scientific), mouse hematopoietic lineage biotin panel (Thermo Fisher Scientific) and SA-APC-Cy7 (#47-4317-82); All data were acquired with a FACSCanto flow cytometer, LSR or LSRII flow cytometer (BD Biosciences) and analyzed using FlowJo v10 software for Windows (Tree Star, Inc.).

Isolation of neutrophils

$CD11b^+Ly6G^+$ neutrophils were isolated from the blood, bone marrow, spleen, lymph node and tumor tissue of untreated or ACT immunotherapy-treated B16F1 tumor-bearing mice. Neutrophils were positively selected from single-cells suspensions by staining with CD45 (Clone 30-F11), Ly6G (both BD Bioscience), CD11b (Biolegend) and sorting with a BD FACSAria II Cell Sorter (BD Biosciences).

T cell conditioned medium (T cell-CM)

For generation of T cell conditioned medium 1×10^6 Pmel-1 T cells were cultured in 24-well plates, stimulated with 1 μg/ml of the $H2\text{-}D^b$ binding peptide KVPRNQDWL ($gp100_{aa25–33}$) and 30cU/ml recombinant human IL-2 (Aldesleukin) in 1 mL complete RPMI medium. T cell supernatants were collected after 18 hours.

3′mRNA-Seq analysis of neutrophils

Neutrophils isolated from the bone marrow as described above were stimulated over night with T cell-conditioned medium (T cell-CM). *In vitro* stimulated or sorted neutrophils from ACT immunotherapy-treated mice were lysed in 200 μL RLT buffer (QIAGEN). Total RNA was isolated using Zymo I spin columns (Zymo Research) and eluted in 8 μL of RNAase-free H_2O. Because the yield of isolated neutrophils differed between tissues, we pooled neutrophils from different mice if necessary: Bone marrow neutrophil samples were from individual mice, spleen neutrophil samples were pools from two mice. Blood, draining lymph node and tumor neutrophil samples were pools from four mice. RNA concentrations were determined using Qubit (LifeTech). Isolation of neutrophils from tumor tissues and draining lymph nodes yielded low numbers of neutrophils. We expected and obtained lower yield and reduced quality RNA from these samples e.g., in comparison to the isolated RNA from bone marrow neutrophils. For this reason, we decided to use a 3′mRNA-seq method for our transcriptome discovery approach that is known to be more robust for RNA of reduced quality. 3′mRNA-seq library preparation was performed using the forward QuantSeq 3′mRNA-Seq Library Prep Kit for Illumina (Lexogen GmbH, Austria) according to the manufacturer's protocol with modifications for low-input and reduced quality input RNA. Depending on the amount of input RNA between 14 or 18 PCR cycles were used for PCR-based library amplification. Size distribution and yield of the 3′mRNA-seq library after the PCR step was determined by the D1000 high sensitivity tape station (Agilent) prior to pooling of the barcoded libraries. The pooled 3′mRNA-Seq libraries were loaded on the Illumina HiSeq2500 platform and analyzed by a 50 cycles rapid run with on-cartridge clustering. Computational 3′mRNA-seq analysis was done with the Bioconductor/R computing environment essentially as outlined: http://bioinf.wehi.edu.au/RNAseqCaseStudy/. FASTQ files were aligned to the mm10 mouse reference genome using the RSubread aligner package. To adjust the alignment procedure for the 3′mRNA-Seq data as suggested by Lexogen, the Rsubread align function was executed without trimming but allowing for mismatches in the initial cycles. Only reads > 45 bases were included in the analysis (minFragLength = 45). Initial mapping with the Rsubread algorithm (align) was done with a relaxed setting allowing for ambiguous mapping (max two genomic sites to allow for junction reads), but the gene level summary method (featureCounts) was done with unique mapping requirement. The final percentage of reads assigned to mRNAs was lower in 3′mRNA-seq libraries prepared from lymph node and tumor neutrophils versus the other samples, because these libraries contained a higher frequency of overrepresented reads (e.g., polyA sequences) favored by the lower input and reduced RNA quality. Therefore, the voom method of the limma package was used for normalization and mRNA expression values were transformed to log2 values of

read counts per million (cpm). The voom normalization method was shown to be robust and reliable when the total read counts per sequenced RNA-seq library differ. Other Bioconductor and R packages used for the analyses and data visualization include (as listed in the key resource table): edgeR, org.Mm.eg.db and heatmap.3.

T cell proliferation and IFN-γ production assay

Antigen-dependent T cell proliferation or IFN-γ production in the presence of neutrophils was assessed by a fluorescent dye dilution assay or intracellular cytokine staining. Antigen specific T cells were isolated from spleens of TCR-transgenic Pmel-1 mice, labeled with 5 μM cell proliferation dye eFluor 670 (eBioscience) according to standard protocols and cultured with neutrophils (ratio 1:1) isolated from the bone marrow or spleens of B16F1 tumor-bearing mice in flat-bottom 96-well plates. Neutrophils from the bone marrow or spleen of C57BL/6 or Nos2-deficient mice were isolated as described above. These co-cultures were stimulated with 1 μg/ml of the H2-D^b binding peptide KVPRNQDWL ($gp100_{aa25–33}$) in complete RPMI medium with 30cU/ml recombinant human IL-2 (Aldesleukin) in the presence or absence of anti-PD-L1 antibody (10 μg/ml; clone:10F.9G2; BioXCell). Antigen-specific T cell proliferation or IFN-γ production was determined by flow cytometry after 72 hours. All data were acquired with a FACSCanto flow cytometer, LSR or LSRII flow cytometer (BD Biosciences) and analyzed using FlowJo v10 software for Windows (Tree Star, Inc.).

PD-L1 upregulation on neutrophils *in vitro*

Neutrophils were isolated from the bone marrow of B16F1 tumor-bearing mice as described above. Neutrophils were cultured in flat-bottom 96-well plates and stimulated with recombinant murine IFN-y (1000 U/ml; Peprotech) or T cell conditioned medium. PD-L1 surface expression on neutrophils was determined by flow cytometry over time. All data were acquired with a FACSCanto flow cytometer, LSR or LSRII flow cytometer (BD Biosciences) and analyzed using FlowJo v10 software for Windows (Tree Star, Inc.).

ELISA

HGF concentrations in sera and tissues from mice were measured using the mouse/rat HGF Quantikine ELISA kit (R&D, cat#MHG00) according to manufacturer's protocols on day 7-10 after start of therapy. In brief, blood was collected from tumor-bearing mice treated as indicated and serum was prepared according to manufacturer's instruction. Tissue proteins were isolated using the M-PER mammalian protein reagent (Fermentas) with protease inhibitors (Thermo Fisher Scientific) and quantified using a BCA protein assay (Pierce, Thermo Fisher Scientific) according to manufacturer's protocol. To determine HGF protein levels in tissues 100 μg protein were analyzed. To measure HGF release of neutrophils, cells were isolated from the bone marrow of B16F1 melanoma-bearing mice as described above. 300.000 neutrophils were plated in flat-bottom 96 well plates and stimulated with LPS (1 μg/ml; Invivogen), recombinant murine IFN-y (1000 U/ml; Peprotech), recombinant murine TNFα (1000 U/ml; Peprotech) or T cell conditioned medium in serum-free RPMI 1640 medium (Thermo Fisher Scientific) supplemented with 2 mM L-glutamine, 10 mM non-essential amino acids, 1 mM HEPES (all from Life Technologies), 20 μM 2-mercaptoethanol (Sigma), 100 IU/ml penicillin and 100 μg/ml streptomycin (Invitrogen) in a humidified incubator with 5% CO_2. After 18 hours HGF concentration in neutrophil supernatants was determined. HGF concentrations in sera from metastatic melanoma patients before and after the 3rd treatment with anti-PD1 immunotherapy were measured using the human HGF Quantikine ELISA kit (R&D, cat#DHG00) according to manufacturer's protocols. Optical density was measured in a microplate reader set to 450 nm (BIOTek).

Immunofluorescence staining of lymph nodes

Tumor draining inguinal lymph nodes from B16F1 tumor-bearing $Ly6G^{Cre}ROSA26^{LSL\text{-}tdTomato}$ mice treated as indicated were harvested on day 10 after adoptive transfer of GFP expressing Pmel-1 T cells and fixed in PLP buffer (0.05 M phosphate buffer containing 0.1 M L-lysine (pH 7.4), 2 mg/ml NaIO4 and 10 mg/ml paraformaldehyde) for 12 hours, then dehydrated in 30% sucrose prior to embedding in OCT freezing media (Sakura Finetek). 30 μm sections were cut on a CM3050S cryostat (Leica), adhered to Superfrost Plus slides (VWR), stained, mounted with Fluormount G (Southern Biotech), and acquired on a 710 confocal microscope (Carl Zeiss Microimaging). Frozen sections were permeabilized and blocked in 0.1M Tris (AppliChem) containing 0.3% Triton X-100 (GERBU Biotechnik), 1% FCS (Biochrom AG), 1% GCWFS (Sigma Aldrich) and 1% normal mouse serum (Life Technologies). GFP expressing Pmel-1 T cells were stained with a rabbit polyclonal anti-GFP-Alexa488 antibody (#A21311; Thermo Fisher Scientific). Serial lymph node sections were prepared, each section was visually inspected using epifluorescent light microscopy and several representative sections from different LN areas were acquired using confocal microscopy for detailed 3D analysis. Further technical details were described previously (Eickhoff et al., 2015).

Quantitative analysis of imaging data

Automated analysis was performed using the Imaris software tools (Eickhoff et al., 2015). Neutrophils and T cell populations were localized using Imaris surface function and T cell populations were localized using Imaris spot function. Quantification of the relative distance (T cell spot to Neutrophil spot) was calculated using Excel software calculating the minimal distance in 3D.

Intravital two-photon imaging

B16F1 tumor-bearing $Ly6G^{Cre}ROSA26^{LSL\text{-}tdTomato}$ mice were anesthetized with isoflurane (Baxter; 2.5% for induction, 1∼1.5% for maintenance, vaporized in a 80:20 mixture of O_2 and air), tumor draining inguinal lymph node were exposed and intravital microscopy was performed. The imaging system was composed of a Chameleon laser (Coherent) tuned to 930nm and a Zeiss 780 upright

microscope equipped with a 20 × water immersion lens (NA 1.0, Zeiss) and ZEN acquisition control software. The microscope was enclosed in an environmental chamber in which anesthetized mice were warmed by heated air and the surgically-exposed inguinal (tumor draining) lymph node was kept at 36-37°C with warmed PBS. For dynamic imaging we typically used a z stack of 57 μm and 3 μm step size and acquired every 40 s. Raw imaging data were processed and analyzed with Imaris (Bitplane).

TCGA transcriptomic analysis

Gene expression data (RNA-seq) of TGCA cancer cohorts was accessed through the cBioportal for Cancer Genomics (http://www.cbioportal.org) using the R-based package CGDS-R and following the TCGA guidelines for the use of TCGA data (https://cancergenome.nih.gov/). We retrieved individual gene expression values for the genes of interest as RPKM normalized read counts. RPKM-values less than 1 were set to 1 to avoid negative expression values upon log2-tranformation. All melanoma samples were ordered by increasing expression values of the averaged neutrophil signature. The following genes were used to build the neutrophil signature: *CD93, CSF3R, FCGR3B, TECPR2, FPR1, S100A12, TNFRSF10C, CYP4F3, CXCR2, CXCR1, FCAR, LILRB2, FPR2, CEACAM3, ALPL, SIGLEC5, VNN3*. The moving average of *HGF* gene expression in tumor tissues was calculated using a sample window size of n = 20 and respective colored trend lines (HGF expression) were added to the barplots (Riesenberg et al., 2015). Significance of non-parametric Spearman rank correlation was determined by an asymptotic Spearman correlation test (coin - R package) using the original log2 expression values and not the moving average values.

QUANTIFICATION AND STATISTICAL ANALYSIS

Statistical analyses

Statistical significance of experimental results was evaluated with GraphPad Prism4 software using the parametric unpaired two-tailed student's t test, Mann-Whitney test, Wilcoxon test, asymptotic Spearman correlation test, log-rank test depending of the type of source data. P values less than 0.05 were considered significant. Raw p values were corrected for multiple comparisons if required using the Benjamini & Hochberg methods (= false discovery rate).

Selection of statistical tests

Tumor area, cell proliferation, white blood cell counts and HGF concentrations were considered as normally distributed values with similar variances. Parametric tests (t test) were used for significance analysis in these cases. Frequencies of cell populations determined by flow cytometry and Neutrophil-to-T cell ratios were compared with non-parametric Mann-Whitney test statistics. Changes in patients' absolute neutrophil blood counts and changes in serum HGF levels were also compared by non-parametric Mann-Whitney test statistics, and correlation between these two parameters by Spearman's rank correlation. Survival probabilities with 95%-CI were calculated according to Kaplan-Meier and compared with long-rank test statistics. Statistical tests were performed with the GraphPad Prism 4 software or the R computing platform and specified in the respective figure legends including their test direction (e.g., unpaired two-tailed Student's t test).

DATA AND SOFTWARE AVAILABILITY

The accession number for the 3′mRNA-Seq data reported in this paper is ENA: ERP023772/PRJEB21513. Bioinformatic analyses were done with standard routine implemented in the R/Bioconductor environment. R-programming code is available on request.